bioRχiv
THE PREPRINT SERVER FOR BIOLOGY

ARTICLE PREPRINT

Protection from liver cancer in a mouse model of Alagille syndrome follows dysregulated differentiation of thymocytes and hepatocytes

Jan Mašek[1,2,3]*, Iva Filipovic[4☯], Simona Hankeová[1☯], Jingyan He[1☯], Noémi Van Hul[1,2], Lenka Belicová[1], Markéta Jirouškova[5], Anna Maria Frontino[2], Fabio Turetti[2], Daniel V. Oliveira[2], Igor Červenka[1], Lenka Sarnová[5], Elisabeth Verboven[1], Tomáš Brabec[2], Niklas K. Björkström[4], Martin Gregor[5], Jan Dobeš[2], Emma R. Andersson[1,3]*
☯equal contribution
Corresponding authors' contact information: * correspondence to jan.masek@natur.cuni.cz and/or emma.andersson@ki.se

Affiliation:
[1] Department of Cell and Molecular Biology, Karolinska Institute, Stockholm, SE-171 77 Solna, Sweden.
[2] Department of Cell Biology, Faculty of Science, Charles University, Viničná 7, 128 00 Prague 2, Czech Republic.
[3] Department of Biosciences and Nutrition, Karolinska Institute, Huddinge 14183, Sweden
[4] Center for Infectious Medicine, Department of Medicine Huddinge, Karolinska Institutet, Karolinska University Hospital, Stockholm, Sweden
[5] Laboratory of Integrative Biology, Institute of Molecular Genetics of the Czech Academy of Sciences, Vídeňská 1083, Prague, Czech Republic.

Keywords: Notch; Jagged1; Alagille; Fibrosis; Lymphocytes; Liver development; Single cell

ABSTRACT

Background and Aims: Alagille syndrome (ALGS) is a pediatric genetic disorder, caused by mutations in the Notch ligand *JAGGED1*, presenting with cholestasis due to intrahepatic bile duct paucity. Despite chronic liver disease, few patients develop severe fibrosis or liver cancer, compared to other chronic liver diseases. In contrast, about 1/3 of ALGS patients suffer from reoccurring infections. Notch signaling regulates both liver and immune system development, but how immune system defects interact with liver pathology in ALGS to influence disease course is not known. Here, we aimed to determine whether a mouse model of ALGS mimics fibrosis and liver cancer, and whether ALGS immune system compromise could positively modulate inflammation or liver disease course.

Methods: We used single cell RNA sequencing and 25-color flow cytometry to characterize cell populations in embryonic and postnatal liver in an ALGS mouse model (*Jag1*$^{Ndr/Ndr}$ mice). We analyzed liver cancer prevalence in *Jag1*$^{Ndr/Ndr}$ mice, in a cancer-prone genetic background, and thymic and spleen cell composition using flow cytometry. Finally, to test the functionality of the *Jag1*$^{Ndr/Ndr}$ immune system we performed adaptive immune cell transfer experiments into *Rag1*-/- mice and assessed inflammatory capacity in an ulcerative colitis model and in a DDC model of hepatocellular damage.

Results: Adult *Jag1*$^{Ndr/Ndr}$ mice do not develop liver tumors (0%) while 45% of control mice do. Interestingly, *Jag1*$^{Ndr/Ndr}$ mice display ALGS-like chicken-wire hepatocellular fibrosis concomitant with mild inflammation shortly after the onset of liver cholestasis. Comprehensive single cell analysis revealed that liver CD4$^+$ and CD8$^+$ T cells of *Jag1*$^{Ndr/Ndr}$ mice are dysregulated in favor of CD4$^+$, and Regulatory T-cells (Tregs) manifest reduced activation. Transplantation experiments show no difference between *Jag1*$^{Ndr/Ndr}$ and *Jag1*$^{+/+}$ lymphocytes in DDC-induced liver damage. In contrast, *Jag1*$^{Ndr/Ndr}$ lymphocytes do not mount an inflammatory response to bacterial infection.

Conclusion: Here we report immune dysregulation and cancer protection in the hypomorphic *Jag1* mouse model of ALGS. Disrupted thymocyte differentiation coincides with limited activation of hepatocytes, blunting the inflammatory response to cholestasis. This may contribute to the pericellular fibrosis and prevent carcinogenesis. These results prompt the question of the relative contribution of Jag1 to liver cell pathology vs immune system in ALGS and highlight the need of future studies focused on dissecting apart how Jag1 modulates susceptibility to infection versus cancer risk.

INTRODUCTION

The adult mammalian liver is a complex metabolic organ with remarkable regenerative capacity, and a crucial role as an immune interface, which is indispensable for whole organism homeostasis. In contrast to its purpose in adulthood, the developing liver serves as a transient hematopoietic niche from its establishment (in mouse Embryonic day (E) 10.5), until early postnatal stages (in mouse postnatal day (P) P7) [1–4]. The shift from one systemic function to the other overlaps with the onset of pediatric cholestatic phenotypes in human congenital cholangiopathies and respective mouse models, reviewed in [5,6]. Liver injury induces inflammation, which can lead to fibrosis, cirrhosis, and ultimately result in hepatocellular carcinoma (HCC), reviewed in [7]. However, little is known of how the neonatal immune system affects liver parenchyma in pediatric liver disease, in particular with respect to long-term outlook and cancer.

The Notch signaling pathway is conserved across metazoan animals, driving stemness, proliferation, differentiation, and decision-making processes, both in development and adulthood, and when disturbed, leads to a variety of developmental diseases and cancer, reviewed in [8,9]. Alagille syndrome (OMIM 118450; ALGS) is a multisystemic pediatric genetic disorder usually caused by mutations in the Notch ligand *JAGGED1* (*JAG1,* 94% of cases) [10–12], or in the NOTCH2 receptor itself (2,5% of cases) [12,13]. ALGS is characterized by bile duct paucity (often resulting in liver transplantation), developmental heart defects, butterfly vertebrae, characteristic facies,

posterior embryotoxon and multiple associated symptoms, including the immune dysregulation, present with different penetrance [8,14,15]. Notch signaling controls development of both liver epithelial cells (hepatocytes and cholangiocytes) [16–20] and the immune cells [21–26] yet how the immune system is affected in ALGS, and its impact on liver disease progression, has not yet been comprehensively addressed.

Notch signaling has been implicated in multiple aspects of liver cancer progression [27–30]. For example, a Notch "ON" signature was found in ~30% of HCC patients (n=144) [27]. However, the specific role for JAG1 in hepatitis, fibrosis, cirrhosis or carcinogenesis is unclear. Both up-regulation [31,32], and down-regulation [33,34] of JAG1 have been implicated in liver cancer, as well as non-canonical JAG1 intracellular domain effects [35]. Although ALGS is thought of as a Notch haploinsufficiency syndrome, until recently it was not clear if the ALGS patients are protected from HCC, or not [36]. Recent GALA report on a large cohort of ALGS patients (n=1433) revealed, the HCC develops in ALGS patients in <1% of cases (n=9/1433, or 0.6%)[37]. By way of comparison, the rate of HCC in pediatric liver diseases ranges from 0.8% in biliary atresia [38], to 2% in Hepatitis B infections, to 14% in Progressive familial intrahepatic cholestasis (PFIC) [39,40], and 13-17% for tyrosinemia type 1 [41]. Further, only 5 out of the 9 ALGS patients with HCC from the cohort of 1433 developed fibrosis [37], which combined with the fact that, despite cholestasis, only ~12-14% of ALGS patients develop cirrhosis [36,42], suggests that JAG1 haploinsufficiency confers, via unknown mechanism, protection against HCC. Interestingly, fibrosis in ALGS, when present, is atypical, with a pericellular "chicken-wire" appearance, rather than bridging fibrosis [43], suggesting the inflammation-fibrosis-cirrhosis-HCC axis is likely disrupted in ALGS, with unclear consequences for progression to HCC. Resolving the role of Jag1 in fibrosis and HCC is thus of importance not only for ALGS, but also for Notch-driven HCC.

Prior to fibrosis and cirrhosis, cholestasis induces inflammation, attracting immune cells to the liver to modulate the disease response. Liver inflammation in cholestasis involves T cells [44–46], Regulatory T-cells (Tregs) [47], natural killer (NK) cells [48,49], invariant NKT (iNKT) cells [50,51], and myeloid cells [28,52,53], most of which are at some point of their development subject to Notch regulation, reviewed in [54]. Notch1 is crucial for thymic development [55], and the T cell lineage specification in liver and thymus [21,22,26], and Jag1 controls Dendritic [56] and NK cell maturation in lymph nodes [57,58] and serves an important bone marrow stromal factor for the long-term hematopoietic stem cells [59]. Disruptions in Notch activity could thus modulate disease progression by determining the capacity for inflammation and immune response, thereby modifying fibrosis and cirrhosis, and the risk of HCC. Importantly, disrupted Jag1 signaling is associated with a ~30% increase in infections in patients with ALGS [15], possibly via a Notch receptor-independent mechanism regulating T-cell function itself [60]. The immune dysregulation in ALGS thus represents an intriguing, yet severely understudied, aspect of the ALGS pathology whose impact on liver disease progression has not been tested yet.

Here, we addressed the developmental and adult roles of Jag1 in the immune system in inflammation, fibrosis, and HCC, using *Jag1*$^{Ndr/Ndr}$ mice, a model of ALGS. *Jag1*$^{Ndr/Ndr}$ mice are maintained in a genetic background which is prone to HCC in wild type conditions, providing an ideal model to investigate the cholestasis/ inflammation/ fibrosis/ cirrhosis/ HCC axis. First, we show that *Jag1*$^{Ndr/Ndr}$ mice do not develop HCC by the age of one year, unlike wild type littermates, but do display ALGS-like pericellular fibrosis. To resolve cell type composition and developmental specification of epithelial and immune cells in embryonic and postnatal liver, we used multi-color FACS and sc-RNA-sequencing of whole liver, identifying delayed differentiation of epithelial cell types, compromised inflammatory capacity, and a reduction in infiltration of lymphocytes (T cells). There were no overt differences in the number or expression profiles in endothelial, mesenchymal, Kupffer, nor NKT cells, suggesting the T-cell function, regulated by Jag1, could modulate the liver pathogenesis. The observed reduction of T cells led us to a discovery of a deregulated development of thymocytes, resulting in overabundance of CD4^{+} and Tregs at the expense of the CD8^{+} T cells with limited activation capacity. To address Jag1-abrogated T-cell function, we used immune transplantation mouse models of autoimmunity, chemically induced cholestasis, and bacterial infection, revealing that *Jag1*$^{Ndr/Ndr}$ lymphocytes are not autoimmune, do not alter the chemically induced fibrotic response, but fail to respond to bacterial infection. These results uncover several new aspects of ALGS pathology linked to roles of Jag1 in hepatic and T cell development, which may help liver cancer.

RESULTS

Hypomorphic Jag1 signaling prevents spontaneous liver cancer development in mice.

Whether loss of Jag1 signaling is protective or detrimental in ALGS, with regards to fibrosis, cirrhosis, and development of liver cancer, is controversial and not yet well understood [31–35]. Forty-eight percent (48%) of wild type C3H x C57bl6 male mice spontaneously develop liver tumors [64], indicating that the genetic background of *Jag1*$^{Ndr/Ndr}$ C3H/C57bl6 mice is ideal for investigating whether Jag1 insufficiency is protective or detrimental[61,62].

We assessed male *Jag1*$^{+/+}$ and *Jag1*$^{Ndr/Ndr}$ C3H/C57bl6 mice at 13 months +/- 2 months. Forty-three percent of *Jag1*$^{+/+}$ male mice developed liver tumors (n=5 of 11), as expected [64], but no tumors were found in the *Jag1*$^{Ndr/Ndr}$ males (n=0 of 9) (**Fig. 1A, A'**). Liver tumors in wild type C3H/C57bl6 mice displayed high cell density of HNF4a+ cells, which were also positive for cytosolic CTNNB1, a marker of activated canonical Wnt signaling, and hallmark of HCC [65] (**Fig. 1B**). JAG1 protein is detectable in both healthy wild-type liver tissue and in *Jag1*$^{Ndr/Ndr}$ livers, since the missense mutant JAG1 is also expressed, but JAG1 is

absent from the tumor area (**Fig. 1C**), suggesting cancer progression is JAG1-independent at this stage.

The data suggest that Jag1-mediated Notch signaling plays a role in processes preceding tumorigenesis. We therefore asked whether cholestatic *Jag1*$^{Ndr/Ndr}$ mice exhibit high levels of fibrosis, as expected based on liver injury, or lower levels of fibrosis with pericellular localization, mimicking ALGS.

Jag1$^{Ndr/Ndr}$ newborns are jaundiced by postnatal day 3 (P3), with persistent high levels of bilirubin at P10, which resolves by adulthood [61,62]. To determine whether cholestasis is associated with fibrosis in *Jag1*$^{Ndr/Ndr}$ mice, we examined Collagen deposition using Sirius red staining at P10. Detailed examination revealed that fibrosis is heterogenous across the liver with both pericellular "chicken-wire" fibrosis (**Fig. 1D- E'**) and in more dense fibrotic loci with pronounced immune cell infiltrate (white arrow heads, **Fig. 1D'', E''**).

Jag1$^{Ndr/Ndr}$ mice are thus protected from spontaneous liver cancer, and display both pericellular and immune-associated fibrosis in response to cholestasis. The atypical and mild fibrotic reaction, and absence of liver cancer, despite severe bile duct paucity and cholestasis [61,62] suggests both liver parenchymal and incoming immune cells are affected by Jag1 haploinsufficiency.

Comprehensive single cell analysis identifies a reduction in T-cells in Jag1$^{Ndr/Ndr}$ mice.

Current knowledge of the cellular interactions regulating fibrosis in pediatric cholestasis is limited, as virtually all mammalian models of intrahepatic cholestasis use adult animals, reviewed in [6,70]. To determine, in an unbiased fashion, whether and how the onset of biliary phenotype affects liver cell populations [61], we analyzed livers of *Jag1*$^{+/+}$, *Jag1*$^{Ndr/+}$, and *Jag1*$^{Ndr/Ndr}$ mice at P3 using 10x genomics sc-RNA-seq and simultaneously characterized the cell populations by their protein expression using multicolor Flow cytometry (**Fig. 2A-A''**). To complement the analysis with a dataset of pre-cholestatic liver, we included embryonic day (E) 16.5, a stage at which the ductal plate is emerging and the liver is undergoing its prenatal function of hematopoiesis [3,16,17,61].

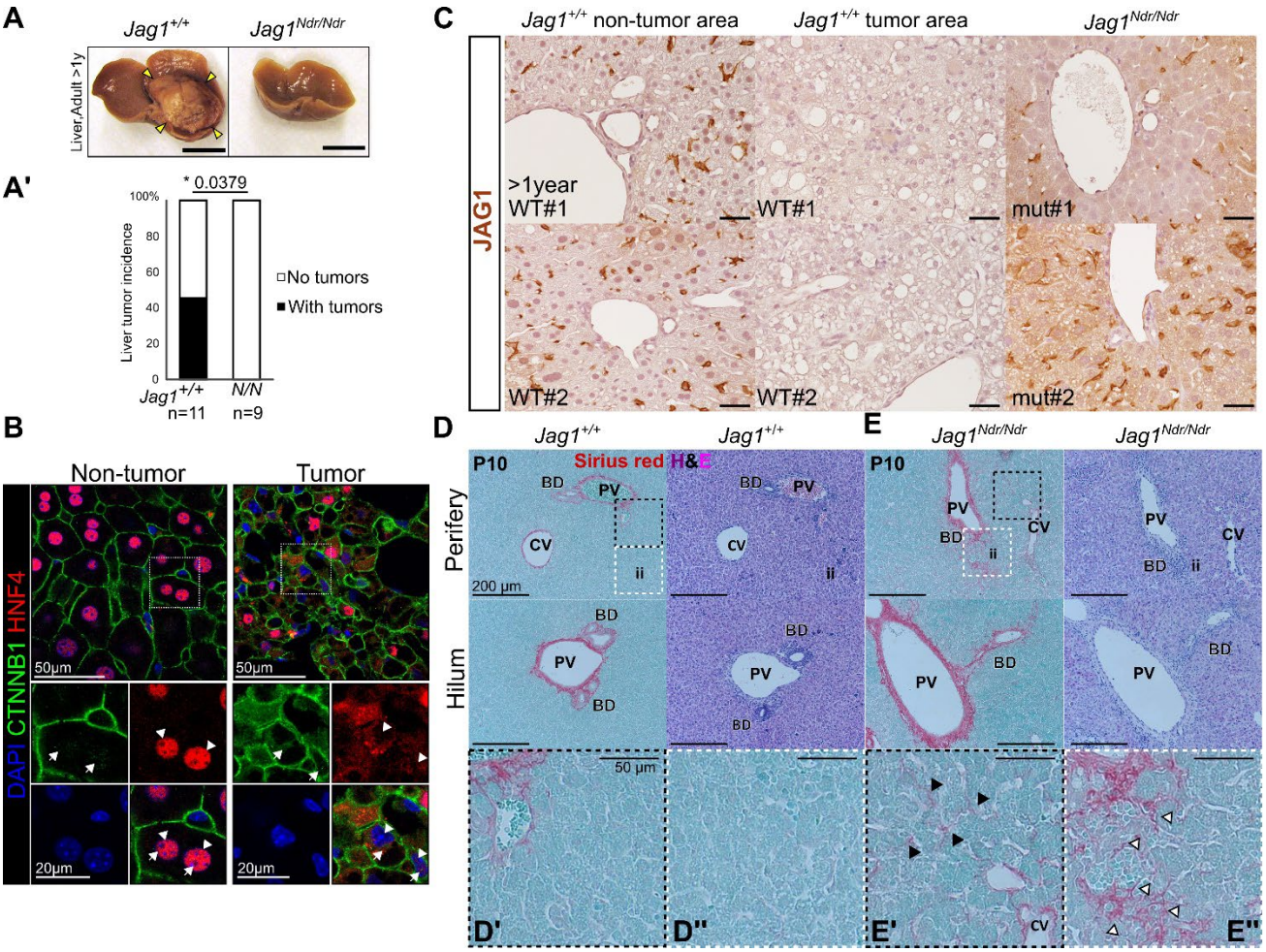

Figure 1: *Jag1*$^{Ndr/Ndr}$ mice display pericellular fibrosis and are protected from developing HCC. (**A**) Example of a spontaneous liver tumor in a C3H/C57bl6 *Jag1*$^{+/+}$ male and a tumor-free liver from a matching *Jag1*$^{Ndr/Ndr}$ male, with corresponding quantification of liver tumor prevalence in male *Jag1*$^{+/+}$ and *Jag1*$^{Ndr/Ndr}$ mice (n refers to individual animals). (**B**) Confocal images of CTNNB1, HNF4α and DAPI staining of non-tumor and tumor liver tissue of >1y old *Jag1*$^{+/+}$ mice. Arrowheads indicate nuclei, and arrows indicate CTNNB1 staining which is cytoplasmic in the tumor. (**C**) JAG1 IHC staining in the *Jag1*$^{+/+}$ non-tumor and tumor area, and in *Jag1*$^{Ndr/Ndr}$ liver of >1y old animals. (**D-E''**) Paraffin sections of liver stained with H&E and Sirius red from *Jag1*$^{+/+}$ (D-D'') and *Jag*$^{Ndr/Ndr}$ (E-E'') animals at P10, with magnified regions depicted by boxing. White arrows denote immune infiltrate. Ndr, Nodder; y, years; CV, central vein; PV, portal vein; BD, bile duct; ii, immune cell infiltrate (not present in control). Fisher Exact test, * = p <0.05.

Analysis of the 2,000 most variable features identified over 20 cell types (depending on the genotype and stage, **Fig. 2B**), which we cross-referenced with reported mouse and human fetal liver sc-RNA-seq [4,72,73] (**Fig. 2C**). As expected, blood lineages (including erythroblasts and erythrocytes) constituted a larger percentage of the cell population in liver at E16.5 (72.7%) than at P3 (28.7%), when the migration of hematopoietic progenitors out of the liver is almost completed (**Fig. S1A**).

The *ex vivo* digest of liver enriched for non-parenchymal cells, enabling analysis of the immune compartment in *Jag1*$^{Ndr/Ndr}$ mice [74]. Most cells belonged to blood cell lineages (~93.5% at E16.5, ~92.5% at P3), while liver parenchymal cells constituted ~6.5% at E16.5, and ~7.5% of the cells at P3 (Fig. S1B). Parenchymal cells include *Pdgfrb*$^{+}$/*Col3a1*$^{+}$/*Dcn*$^{+}$ mesenchymal cells, *Flt4*$^{+}$/*Igfbp7*$^{+}$/*Lyve1*$^{+}$/*Cdh5*$^{+}$ endothelial cells, *Fabp1*$^{+}$/*Apoa1*$^{+}$/*Fgb*$^{+}$/*Alb*$^{+}$ hepatocytes and hepatoblasts, expressing also *Dlk1,* and *H19*. There were few *Sox9*$^{+}$/*Epcam*$^{+}$ cholangiocytes (**Fig. S3 B**) and no smooth muscle cells.

The non-parenchymal cells included tissue-resident macrophages, such as *Vcam1*$^{+}$/*Clec4c*$^{+}$/*Marco*$^{+}$ Kupffer cells, as well as blood cell lineages derived from *Cd27*$^{+}$/*Kit*$^{+}$/*Cd34*$^{+}$ hematopoietic stem cells/erythroid-myeloid progenitors (HSc/EMP), which diverge into the three major paths of differentiation: i) the Myeloid lineage including: *Cd74*$^{+}$/*Clec9a*$^{+}$/*H2-*

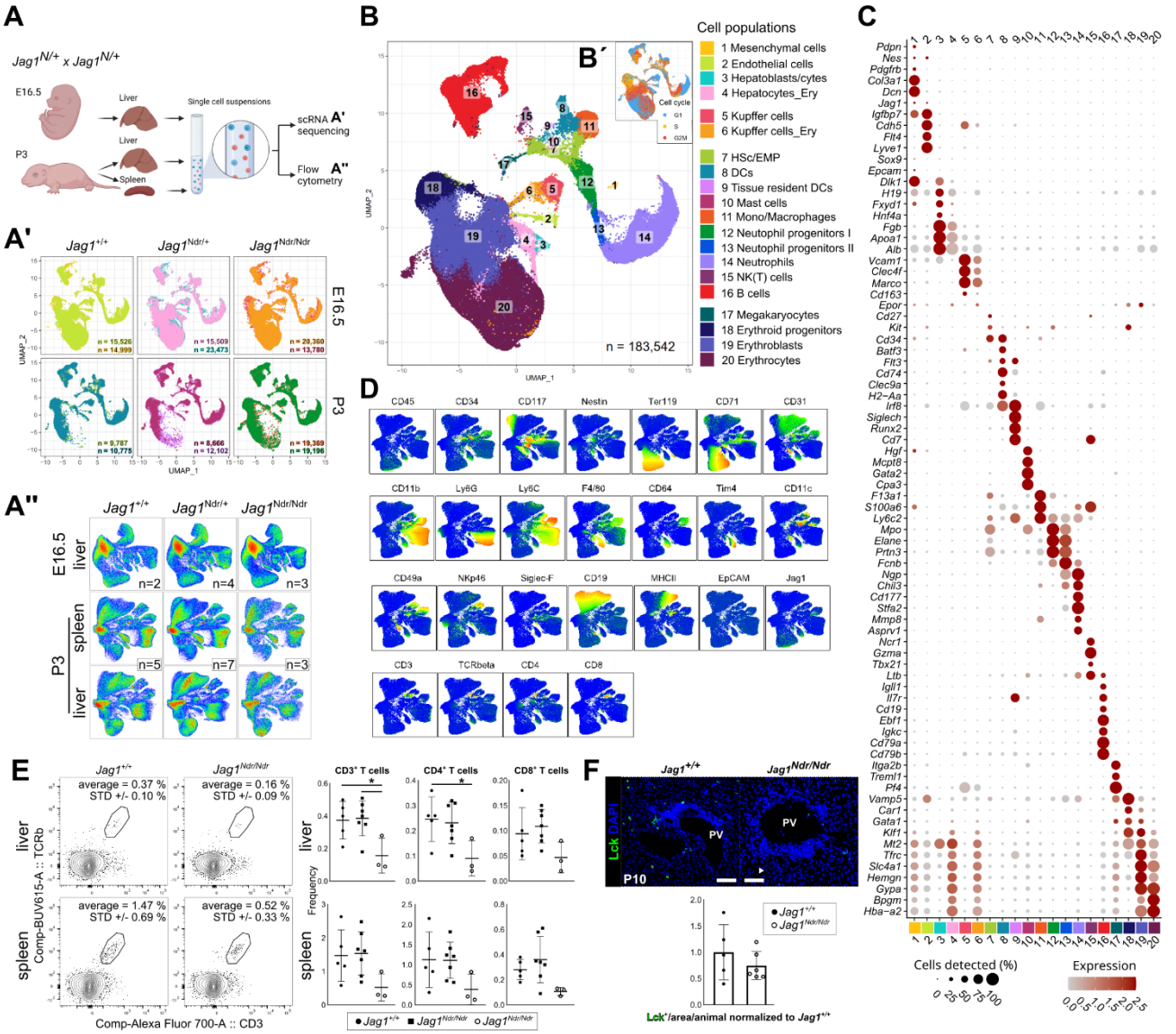

Figure 2: Single cell characterization of cell proportions in *Jag1*$^{Ndr/Ndr}$ mice reveals a reduction in T-cells in *Jag1*$^{Ndr/Ndr}$ liver. (**A-A''**) Scheme of the experiments. A. Composition of the scRNAseq (A') and Flow cytometry (A'') samples including spleen and/or liver from E16.5 and P3 *Jag1*$^{+/+}$, *Jag1*$^{Ndr/+}$, and *Jag1*$^{Ndr/Ndr}$ mice. (**B, B'**) UMAP projection of the 183,542 sequenced cells with clusters assigned to the individual identified cell types, and cell cycle phase (B'). (**C**) Dot plot of the SCT-normalized marker mRNA expression of 78 DEGs characteristic for the individual cell types identified in B. (**D**) UMAP projections of the cells expressing marker proteins across the aggregated 25-colour Flow cytometry dataset of 190,000 cells/sampled from E16.5 and P3 livers, and P3 spleens of *Jag1*$^{+/+}$(n=7), *Jag1*$^{Ndr/+}$(n=11), and *Jag1*$^{Ndr/Ndr}$ (n=6) animals. (**E**) Representative FACS plot of and relative frequency of the CD3^{+}, CD3^{+}CD4^{+}, and CD3^{+}CD8^{+} T cells in liver and spleen of the *Jag1*$^{+/+}$, *Jag1*$^{+/Ndr}$ and *Jag1*$^{Ndr/Ndr}$ at P3, based on the Flow cytometry data (Full data in Fig. S2). (**F**) Representative immunohistochemical staining and quantification of Lck^{+} T cells in periportal area on cryosections from *Jag1*$^{Ndr/Ndr}$ and *Jag1*$^{+/+}$ livers at P10 (4-6 ROI per *Jag1*$^{Ndr/Ndr}$ (n=6 individual animals) and *Jag1*$^{+/+}$ (n=5 individual animals) liver). PV, portal vein; (mean ± SD, one-way ANOVA with Dunnett's multiple comparison test, $p \leq 0.05$ = *)

Aa^{+}/*Irf8*$^{+}$/*Siglech*$^{+}$/*Runx2*$^{+}$/*CD7*$^{+}$ Dendritic cells (DCs), *F13a1*$^{+}$/*S100a6*$^{+}$/*Ly6c2*$^{+}$ Macrophages, *Mpo*$^{+}$/*Elane*$^{+}$/*Prtn3*$^{+}$/*Fcnb*$^{+}$/*Ngp*$^{+}$/*Chil3*$^{+}$ Neutrophil progenitors I and II, *Cd177*$^{+}$/*Stfa2*$^{+/}$*Mmp8*$^{+}$/*Asprv1*$^{+}$ Neutrophils, *Mcpt8*$^{+}$/*Gata2*$^{+}$/*Cpa3*$^{+}$ Mast cells; ii) the Lymphoid lineage *Ltb*$^{+}$/*Igll1*$^{+}$/*Il7r*$^{+}$/*Cd19*$^{+}$/*Ebf1*$^{+}$/*Igkc*$^{+/}$*Cd79a/b*$^{+}$ B-cells; and iii) Erythroid cells including *Car1*$^{+}$/*Gata1*$^{+}$/*Klf1*$^{+}$ progenitors, *Mt2*$^{+}$/*Tfrc*$^{+}$/*Slc4a1*$^{+}$/*Hemgn*$^{+}$ Erythroblasts, *Gypa*$^{+}$/*Bpgm*$^{+}$/*Hba-a2*$^{+}$ Erythrocytes, and *Itga2b*$^{+}$(*Cd41*$^{+}$)/*Treml1*$^{+}$/*Pf4*$^{+}$ Megakaryocytes. The scRNA seq also revealed the presence of population of *Ncr1*$^{+}$/*Gzma*$^{+}$/*Tbx21*$^{+}$ NK(T) cells, coming from both fetal thymus and liver [4,75–78] (**Fig. 2B, C**).

Between E16.5 and P3, there is a dramatic shift in the relative proportions of different liver cell types, with a ~75% decrease in the relative presence of erythrocytes (from ~45% to ~10% of all analyzed cells), accompanied by a corresponding enrichment of the Myeloid lineage (mainly Neutrophilic from 6.6% to 21.0% at P3) and B-cells (from 7.5% to 18.0% at P3) (**Fig. S1C**). There were few or no overt differences in cell type ratios in *Jag1*$^{+/+}$, *Jag1*$^{Ndr/+}$, and *Jag1*$^{Ndr/Ndr}$ livers as identified by the scRNA sequencing at E16.5 or P3 (**Fig. S1B, C**).

To complement the transcriptomic scRNAseq analysis with a method focused on immune cells and protein, rather than mRNA, we applied 25-color flow cytometry [79]. The panel of 25 antibodies included markers of blood lineages, EPCAM^{+} cholangiocytes, NESTIN^{+} mesenchymal cells, and CD31^{+} endothelial cells, and co-staining for JAG1 to identify which cell types express JAG1 (**Fig. 2, A, A'', D)**. Unsupervised clustering of E16.5 and P3 whole liver and P3 splenic cell suspensions from *Jag1*$^{+/+}$, *Jag1*$^{Ndr/+}$, and *Jag1*$^{Ndr/Ndr}$ mice identified 34 different cell populations (**Fig. 2A'', S2 A-C**).

Populations significantly enriched in the *Jag1*$^{Ndr/Ndr}$ mice included CD19^{+}/MHCII^{-} B-cell progenitors (Cluster 9), and CD49a^{+}/Nestin^{+} mesenchymal cells (Cluster 32) present almost exclusively in the E16.5 liver samples, and ALL^{-} cells that we could not identify (Cluster 33) (**S2B, C**). Additionally, we detected the MHCII^{+} B cells (Cluster 5, consistent with changes observed in the scRNAseq (**Fig. S1D**)), and CD4^{+} and CD8^{+} T cells to down-regulated populations, to be underrepresented in the *Jag1*$^{Ndr/Ndr}$ compared to controls (**Fig. 2E** and **S2B, C**).

While there is no clear link between the B cells and the early events in the postnatal cholestasis [80], multiple studies identified different subtypes of T and NKT and NK cells to be the major source of pre- and fibrotic liver damage, rather than the high bile concentration [44,47,81–84]. Surprised by the scarcity of CD4^{+} and CD8^{+} T cell counts in *Jag1*$^{Ndr/Ndr}$ animals (**Fig. 2E**), we wondered if this is a transient or systemic change, specific for the periportal loci of the cholestatic injury. We thus stained and quantified the T cell presence in the periportal areas using Lck antibody recognizing both CD4^{+} and CD8^{+} T cells [85] on cryosections from *Jag1*$^{Ndr/Ndr}$ (n=6), and *Jag1*$^{+/+}$ (n=5) left lateral lobes at P10. Surprisingly, despite the ongoing cholestasis, there was no significant enrichment of Lck^{+} T cells in *Jag1*$^{Ndr/Ndr}$ portal areas compared to *Jag1*$^{+/+}$ controls (**Fig. 2F**).

The unbiased analysis of the pre- and neo-natal liver and splenic tissue revealed a previously unrecognized immune aspect of ALGS-like cholestasis in the mouse model. The T cell deficiency in the periportal liver compartment indicates that either the *Jag1*$^{Ndr/Ndr}$ hepatocytes fail to attract the T cells, the T cells are insensitive to the hepatic chemoattraction, or both.

Delayed hepatocyte maturation, and diminished hepatocyte activation in response to cholestatic injury, in Jag1$^{Ndr/Ndr}$ *mice*

How the pediatric liver responds to cholestasis during the pediatric hematopoietic to metabolic shift [2,4] is poorly understood. In the adult cholestatic liver, bile acids activate hepatocytes, which then secrete cytokines to attract lymphocytes [81]. Liver fibrosis is generated by Hepatic Stellate cells (HSCs) [88–90], and is attenuated by Kupffer cells [50]. To determine whether hepatocytes are activated in *Jag1*$^{Ndr/Ndr}$ mice and can attract lymphocytes, we investigated hepatoblast and hepatocyte populations prior to and after the onset of cholestasis in *Jag1*$^{Ndr/Ndr}$ mice.

Jag1$^{Ndr/Ndr}$ mice do not develop mature bile ducts by P10 [61], but Jag1 is not thought to impact on hepatoblast to hepatocyte differentiation. We subset the 3,803 Hepatoblasts/cytes and Hepatocyte_Ery cells from Fig. 2B, C, and identified different hepatoblast and hepatocyte states in the pre-and postnatal stages (**Fig. 3A**). A substantial portion of cells isolated at E16.5 (78.2%) were *Cd24a*$^{+}$/*Gypa*$^{+}$/*Car2*$^{+}$/*Afp*^{low}/*Alb*^{low}/*H19*^{low}/*Dlk1*^{low} Hepatocyte_Ery cells, likely reflecting the hematopoietic nature of the organ at this stage and possible contamination of cells by erythrocyte lysis. The remainder consisted of *Hnf4a*^{low}/*Afp*$^{+}$/*Alb*$^{+}$/*C3*$^{+}$/*H19*$^{+}$/*Dlk1*$^{+}$ Hepatoblasts (16.8%), and mature *Fabp1*$^{+}$/*Chchd10*$^{+}$/*Hnf4a*$^{+}$/*H19*$^{-}$/*Dlk1*$^{-}$ Hepatocytes (4.9%). There was also a small fraction of *Ebf1*$^{+}$/*Cd79*$^{+}$/*Fabp1*$^{+}$/*Chchd10*$^{+}$/*H19*$^{-}$/*Dlk1*$^{-}$ Hepato_Bcells (0.1%), which are either doublets or could include hepatocyte/B-cell emperipolesis. The P3 composition of cells, with 25.0% Hepatoblasts, 47.1% Hepatocytes, 5.3% Hepato_Bcells (and only 22.5% Hepatocyte_Ery cells) reflects the shift towards metabolic specialization of the neonatal liver (**Fig. 3B-D, S3A, B**).

Cell type ratios were similar in *Jag1*$^{Ndr/Ndr}$, *Jag1*$^{+/+}$, and *Jag1*$^{Ndr/+}$mice at E16.5, but at P3 there were more Hepatoblasts (28.0%), Hepato_Ery (37.2%), and Hepato_Bcells (8.3%), but fewer Hepatocytes (26.5%) in the *Jag1*$^{Ndr/Ndr}$ livers compared to *Jag1*$^{+/+}$ (19.2%; 10.7%; 3.1%; 67.0%) and *Jag1*$^{Ndr/+}$ livers (25.5%; 10.5%; 61%; 2.9%) (**Fig. 3D**). The differences at P3 suggest hampered differentiation of hepatocyte progenitors, which could affect their capacity to become activated upon cholestatic injury.

At P3, the cells identified as hepatoblasts express *Afp*, *Alb*, and *C3* but are *Dlk1*$^{-}$/*H19*$^{-}$, with lower expression of hepatocyte marker genes *Hnf4, Chchd10 and Fabp1* (**Fig. 3B, S3B**), in line with previous reports [4]. To assess whether these differences correlate with the emergence of liver zonation, we analysed the expression of portal (*Sds*, *Cyp2f2*, *Alb*), intermediate (*Hpx*, *Hamp*, *Gsta3, Lect2*), and central (*Gulo*, *Cyp2e1*, *Glul*) zonation markers [91,92] at P3

(**Fig. 3E**). Interestingly, the distribution of zonation markers mirrored the differentiation trajectory of the hepatoblasts (neonatal hepatocytes) towards hepatocytes, assessed with monocle3 [93] (**Fig. S3C**). This suggests delayed hepatoblast-to-hepatocyte differentiation in *Jag1*$^{Ndr/Ndr}$ mice occurs when liver zonation is emerging.

To determine whether the differentiation defect in the *Jag1*$^{Ndr/Ndr}$ hepatocyte lineage is intrinsic, or secondary to cholestasis, we analyzed individual genotypes before and after the onset of cholestasis and performed DGEA (**Fig. S3D**). We grouped Hepatoblasts, Hepatocytes and Hepato_Bcells ("Hepatoblast/cytes") and analyzed the Hepato_Ery cell cluster separately.

Prior to cholestasis, at E16.5, there were 47 up- and 48 down-regulated genes in *Jag1*$^{Ndr/Ndr}$ Hepatoblast/cytes compared to *Jag1*$^{Ndr/+}$ and 14 up- and 31 down-regulated genes compared to *Jag1*$^{+/+}$ controls. At P3 there were 64 up- and 50 down-regulated genes in *Jag1*$^{Ndr/Ndr}$ Hepatoblast/cytes compared to *Jag1*$^{Ndr/+}$, and 36 up- and 15 down-regulated compared to *Jag1*$^{+/+}$ controls (**Fig. 3F, G Table TS1**). We cross-referenced differentially expressed genes to identify those that were corroborated by being dysregulated in multiple comparisons. We identified 14 genes upregulated in two comparisons or more, and 27 genes downregulated in two comparisons or more (**Fig. 3F, G**). Hemoglobin-related genes were upregulated in *Jag1*$^{Ndr/Ndr}$ Hepatoblasts/cytes in multiple comparisons, likely due to contamination from excess erythrocytes in *Jag1*$^{Ndr/Ndr}$ livers (see also **Fig. S1D**).

Noteworthy upregulated genes include *Azgp1* and *Cyp4a14,* while downregulated genes included *Ttr*, *Fos*, *Jun* and *Egr1* (Fig. 3F). Azgp1 is a negative regulator of liver and pancreatic cancer progression, and inhibits TGFβ-driven epithelial to mesenchymal transition [100,101]. *Cyp4a14* (cytochrome P450 omega-hydroxylase 4a14), a marker of cholestasis [102] that counteracts fibrosis [103] was upregulated in *Jag1*$^{Ndr/Ndr}$ hepatocyte populations at P3 (**Fig. 3F, G**). The *Cyp4a14* upregulation at P3 likely indicates some hepatocyte activation due to cholestasis, while *Azgp1* overexpression could repress Tgf-β and contribute to hepatoblast differentiation defects, which is also corroborated by reduced expression of *Ttr* in *Jag1*$^{Ndr/Ndr}$ Hepatoblasts/cytes, a marker of mature hepatocytes.

Fos and *Jun* transcription factors are prominent effectors of TGFβ signaling that promote hepatoblast differentiation [73,94–96] and tumorigenesis [97], and were downregulated in E16.5 *Jag1*$^{Ndr/Ndr}$ hepatoblasts, possibly reducing their differentiation potential (**Fig. 3F,G**). GO GSEA analysis with clusterProfiler [98], confirmed downregulation of SMAD signaling (TGFβ/Fos/Jun dependent [99]), along with proteolysis and metabolism-reducing gene sets in *Jag1*$^{Ndr/Ndr}$ hepatocyte populations at E16.5 (**Fig. S4A-B, S6A, B**).

To better map the onset of the pathology, we employed GO GSEA analysis of significantly dysregulated genes in *Jag1*$^{Ndr/Ndr}$ Hepatoblasts/cytes and Hepatocyte_Ery populations vs. *Jag1*$^{+/+}$, and vs. *Jag1*$^{Ndr/+}$ at P3. This analysis identified elevated metabolic activity, immune processes, immune system development, and hemo-, myelo- and erythro-poiesis in *Jag1*$^{Ndr/Ndr}$ mice. The degree of enrichment is milder in *Jag1*$^{Ndr/Ndr}$ mice compared to *Jag1*$^{Ndr/+}$ mice than when compared to *Jag1*$^{+/+}$ mice (**Fig. S5A-B, S5B, C**), which could explain the lack of overlapping downregulated genes at P3.

We next asked whether the lack of lymphocyte enrichment in cholestatic *Jag1*$^{Ndr/Ndr}$ livers could be due to a failure in hepatocyte activation. We examined the expression of proinflammatory molecules secreted by activated hepatocytes, including downstream targets of profibrotic *Egr1* [81], which was downregulated at E16.5 but upregulated at P3 (**Fig. 3G**). Targets include fibrosis-modulating fibrinogen α chain *Fga* [104,105], and antiphagocytic *Cd47* [106–108]. *Cd47* and *Fga* were, similar to *Egr1*, downregulated at E16.5 (**Fig. 3G, H**), but upregulated at P3 in *Jag1*$^{Ndr/Ndr}$ hepatocytes (**Fig. 3H**). In contrast, effector cytokines and other proinflammatory molecules were either absent or present in very low quantities (**Fig. 3H**).

Since hepatocyte activation was low in *Jag1*$^{Ndr/Ndr}$ mice, it was not surprising that we did not detect any transcriptional changes in fibroblasts, mesothelial cells (**Fig. S6A-H'**), endothelial cells (including portal vascular endothelial cells and LSECs) (**Fig. S7I-O**), Kupffer cells (**Fig. S8A-G**), or NK(T) cells (**Fig. S9A-H**).

To determine whether hepatocyte differentiation is delayed at later stages in *Jag1*$^{Ndr/Ndr}$ mice, we re-analyzed previously reported bulk RNA sequencing data from *Jag1*$^{Ndr/Ndr}$ and *Jag1*$^{+/+}$ P10 livers [61] (**Fig. S3E**). To achieve cell type resolution, we deconvolved bulk RNA-seq data using multi-subject single-cell deconvolution (MuSiC) [109] with a reference scRNA-seq dataset of neonatal P1, P3, P7 liver cell populations [4]. We identified the four abundant cell types in the liver: Hepatocytes, Hepatic stellate cells, Macrophages, and Erythrocytes, with the latter three being enriched in *Jag1*$^{Ndr/Ndr}$ livers. The erythrocyte enrichment also corroborates the interpretation of excess erythrocytes explaining the over-abundance of the Erythroid mRNA footprint in *Jag1*$^{Ndr/Ndr}$ samples (**Fig. 3I**). Enrichment of Hepatic stellate cells aligns with the mild but detectable fibrosis in P10 livers (**Fig. 1D-E**''). We assessed hepatocyte maturity compared to P1, P3, P7 hepatocytes in scRNAseq data. As expected, the majority of the control hepatocytes at P10 (70%) shared an expression pattern with the P7 reference. However, quite strikingly, over 90% *Jag1*$^{Ndr/Ndr}$ hepatocytes expressed a P3 hepatocyte signature (**Fig. 3J**), corroborating that hepatocyte differentiation is delayed in *Jag1*$^{Ndr/Ndr}$ liver until at least P10.

Finally, we used an orthogonal approach to assess hepatocyte activation, using the P10 bulk RNAseq data. The proinflammatory gene *Egr1* (1.0 fold), and a small subset of its downstream targets *Cxcl1* (2.4 fold), *Cxcl2* (2.0 fold), *Cxcl10* (1.8 fold), *Ccl2* (2.2 fold), *Serpine1* (2.7 fold), *Isg20* (1.2 fold), and *Plaur* (1.5 fold) were weakly but significantly elevated in *Jag1*$^{Ndr/Ndr}$ mice (**Fig. 3K, S3F**). This corresponds well with the scattered immune infiltration reported in Fig. 1 E-E'' and confirms that hepatocyte activation is weak at this stage (**Fig. S3G**).

In sum, the insufficient Jag1 signaling of the *Jag1*$^{Ndr/Ndr}$ mutants leads to Tgf-β signaling downregulation, possibly in an Azgp1-dependent fashion, limiting the speed of hepatoblast differentiation. The GO GSEA analysis, together with increased presence of B cells and Erythrocytes suggests hematopoiesis, and liver development are both delayed in *Jag1*$^{Ndr/Ndr}$ mice. Finally, hepatocytes at P3 show the first signs of activation, judged by the elevated levels of *Cyp4a14*, *Egr1*, *Fga*, and *Cd47* but the reaction is mild and fails activate the liver population of NK(T) cells, normally active in response to cholestasis[44,47,81–84], suggesting a limited ability of the *Jag1*$^{Ndr/Ndr}$ hepatocytes to attract T cells.

Disrupted thymic development, splenomegaly and altered T cell differentiation precede cholestasis in Jag1*$^{Ndr/Ndr}$ *mice.

The decrease in CD4^{+} and CD8^{+} T cell populations in liver could result from purely a lack of liver chemoattraction but could also be caused by defects in T cell development.

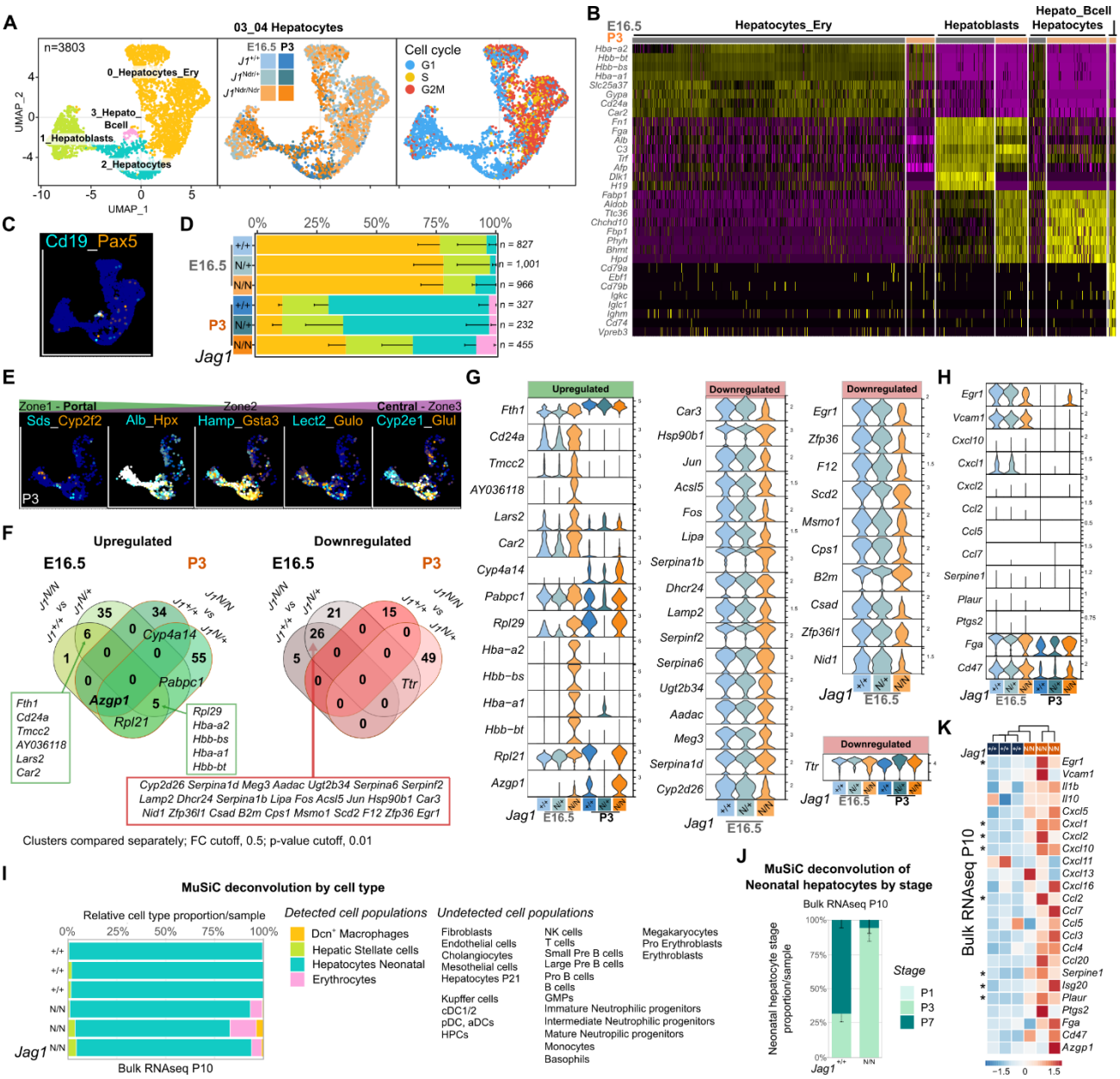

Figure 3: Hepatocyte differentiation is delayed in *Jag1*$^{Ndr/Ndr}$ mice, reducing their potential to become activated by cholestasis. (**A**) UMAP projections of the 03 Hepatoblast/cytes and 04 Hepatocytes_Ery cells subsets, reflecting the subclusters, genotypes and developmental stage, and cell cycle status (**B**) Heatmap of the top 8 marker mRNAs of each cluster at E16.5 and P3. (**C**) Feature plot of *Cd79a*, *Pax5* mRNA expression. (**D**) Average proportion of hepatic cell types per stage and genotype normalized to the number of cells per sample. (**E**) UMAP projections with mRNA expression of zonation markers in P3 data. (**F**) Venn diagrams of differentially expressed genes in *Jag1*$^{Ndr/Ndr}$ vs. *Jag1*$^{Ndr/+}$ and *Jag1*$^{Ndr/Ndr}$ vs. *Jag1*$^{+/+}$ Hepatoblast/cytes. (**G**) Violin plots of the overlapping genes (from F) up- and down-regulated in *Jag1*$^{Ndr/Ndr}$ Hepatoblasts/cytes. (**H**) Violin plots of the selected Egr1-induced proinflammatory genes expressed by activated hepatocyts in *Jag1*$^{Ndr/Ndr}$ and control animals at E16.5, P3 stages. (*Egr1* data for E16.5 is also presented in G). (**I**, **J**) Whole liver cell populations (I), and stage-specific hepatocyte expression profile (J) detected in the bulk RNA seq data from the P10 whole liver of 3 *Jag*$^{Ndr/Ndr}$ and 3 Jag1$^{+/+}$ animals from Andersson et al., 2018, after deconvolution with MuSIC, using scRNA seq data from Liang et al., 2022 as reference. (**K**) Heat map of the selected Egr1-induced proinflammatory genes expressed by activated hepatocytes in *Jag1*$^{Ndr/Ndr}$ and control animals at P10 stage. (Significantly upregulated genes are marked by *, $p_{adj} < 0.01$, $|FC| > 1$).

Unlike the B cell, myeloid and erythroid lineages, T cells develop in the thymus, passing through the liver only briefly (~E12.0 in mouse) as NOTCH1 activation specifies the T from B cell lineages from the common progenitor [21,22,26]. To assess the hematopoietic progenitor populations developmentally regulated by Notch signaling [23–25,110], we used flow cytometry and analyzed the first waves of definitive immune cell production prior to the emergence of the liver (**Fig. S10A, B**). There was no significant difference in populations of Erythroid (Ter119$^+$), Macrophage (Ter119$^-$/cKit$^+$/FcRγ$^+$), Megakaryocyte (Ter119$^-$/CD41$^+$), or Erythro-myeloid (Ter119$^-$/cKit$^+$/FcRγ$^+$/CD41$^+$) progenitor cells from dissociated YSs (**Fig. S10C**) or whole *Jag1*$^{Ndr/Ndr}$ (n=7), *Jag1*$^{Ndr/+}$ (n=9), and *Jag1*$^{+/+}$ (n=8) embryos (**Fig. S10D**) at E9.5.

To discern whether the thymic role of Notch [118][113–117][111,112][55] underlies the T cell deficiency in the cholestatic liver (**Fig. 2E, S2B, C, Fig. 4 L, L'**) we analyzed the developing thymus and its key cell populations before and during cholestasis. First, we mapped the expression of Notch components in human and mouse developing thymus using a published scRNAseq atlas of thymic development [119], confirming the reported expression of *Jag1* in the Thymic Epithelial Cells (mTEC) population, and the brief window of Notch1-mediated activation of the double negative CD3+CD4-CD8- (DN) cells [55,111,112,117,118] (**Fig. 4 A, A'**). Next, we compared the weight of the thymi and spleens of the pre-cholestatic *Jag1*$^{Ndr/Ndr}$ and control neonatal mouse at P0 and cholestatic and control animals at P10 stage. *Jag1*$^{Ndr/Ndr}$ thymi were significantly smaller compared to *Jag1*$^{+/+}$ thymi at P0, a difference that was exacerbated with age (**Fig. 4 B, C**). While the splenic size difference was not significant at P0, at P10 the *Jag1*$^{Ndr/Ndr}$ pups displayed a significant enlargement of the spleen (**Fig. 4C'**).

In mouse, the thymus reaches maturity around P30 [119]. To analyze the final outcome of hypomorphic Jag1 signaling on thymic development, and any basis for immunodeficiency, we dissociated and analyzed thymi from *Jag1*$^{Ndr/Ndr}$ and *Jag1*$^{+/+}$ animals at P30 with flow cytometry. To determine whether Jag1 affects the same processes as Notch1 in TEC development [111,112], we compared the populations of Aire$^+$ mTECs, postAire mTECs, mTECs^{low} (MHCII^{low}CD80^{low}), and mTECs^{high} (MHCII^{high}CD80^{high}), but found no significant difference between *Jag1*$^{Ndr/Ndr}$ (n=6) mice and *Jag1*$^{+/+}$ controls (n=10) at P30 (**Fig. 4D**).

We then explored T cell differentiation, focusing on the populations of DN, CD4$^+$CD8$^+$ double positive (DP), and

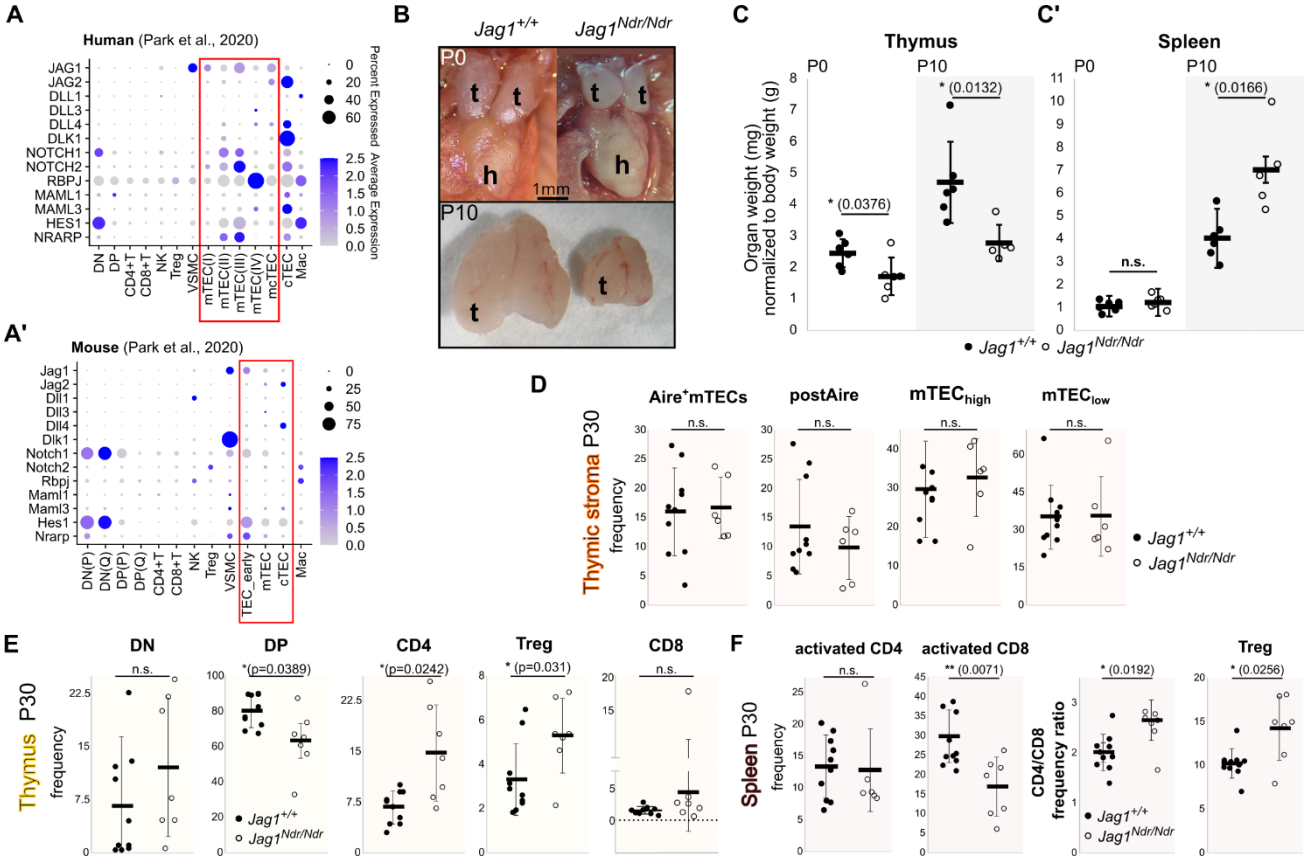

Figure 4: **Enrichment of CD4$^+$ and Treg cells at the expense of cytotoxic CD8$^+$ cells leads to immunodeficiency in *Jag1*$^{Ndr/Ndr}$ mice.** (**A, A'**) Dot plot of the median scaled ln-normalized mRNA expression of Notch signaling components in thymic cell populations (median expression from across the thymic development, data from Park et al., 2020 from human (A) and mouse (A'). (**B**) Macroscopic images of *Jag1*$^{+/+}$ and *Jag1*$^{Ndr/Ndr}$ thymi at P0 and P10. (**C, C'**) Thymic (C) and splenic (C') organ weight at P0 and P10, normalized to the total body weight of the mice (*Jag1*$^{+/+}$ n=6 per genotype and stage and *Jag1*$^{Ndr/Ndr}$ thymus n=6 per genotype and stage; spleen n=5 per genotype and stage.) (**D-F**) Flow cytometry analysis of cell frequencies of different thymic TEC (D), T cell (E), and splenic T cell (F) populations isolated from *Jag1*$^{+/+}$ (n=10) and *Jag1*$^{Ndr/Ndr}$ (n=7) mice at P30. (mean ± SD, Statistical analysis was performed by unpaired, two-tailed Student's t-test, $p \leq 0.05$ = *, $p \leq 0.01$ = **, n.s. not significant). t, thymus; h, heart; s, spleen; DN, Double Negative (CD3$^+$CD4$^-$CD8$^-$); DP, Double Positive (CD4$^+$CD8$^+$); TEC, Thymic Epithelial Cell

CD4$^+$ T cells, CD4$^+$/Foxp3$^+$ Treg cells, and CD8$^+$ T cells in the thymus. While there was no significant difference in frequency of the DN cells, there were significantly fewer DP cells, suggesting the ratio of differentiation is skewed in *Jag1$^{Ndr/Ndr}$* animals. This is further reflected by the significantly enriched differentiation into CD4$^+$ and T reg cells (**Fig. 4E**). The frequency of the CD8$^+$ cells was highly variable (**Fig. 4E**), and there was no change in the CD4$^+$/CD8$^+$ ratio (data not shown) in the thymus. We then investigated mature T-cells in the spleen and found a significant decrease in the frequency of activated CD8$^+$/CD44$^+$ cells, likely reflecting the shifted ratio of CD4$^+$ and CD8$^+$ frequencies in favor of CD4$^+$, accompanied by the overabundance of Tregs (**Fig. 4F**).

Collectively, these data revealed a previously unreported role for Jag1 in thymic development in a model for ALGS, which precedes cholestasis. Defective *Jag1^{Ndr}* signaling results in overabundance of CD4$^+$ and Treg cells at the expense of the CD8$^+$ T cells, with limited activation potential in the secondary lymphoid organ, the spleen.

Jag1$^{Ndr/Ndr}$ T cells do not affect experimentally induced fibrosis but are immunodeficient.

Lymphocyte activity can be modulated by Jag1 expressing hepatocytes, which induce Notch1-mediated production of proinflammatory IL10 in Th1 cells [123]. Further, a Notch-independent interaction between Jag1 and CD46 directly activates IFN-γ/IL-10 production in Th1 cells [60]. To test whether *Jag1$^{Ndr/Ndr}$* T cells were fully competent but did not receive the required signal in the liver, or if they were intrinsically dysfunctional, we performed adaptive transfer experiments of lymphocyte populations into *Rag1$^{-/-}$* mice, a common mouse model deficient for mature B and T cells [124]. The transfer of T-cells to lymphodeficient recipients leads to mild inflammation in the gastrointestinal tract, serving as a useful sensor of hyper- or hypo-active T cells [125,126].

After the transfer, we recorded *Rag1$^{-/-}$* mouse weight gain, receiving the *Jag1$^{Ndr/Ndr}$*, and *Jag1$^{+/+}$* lymphocytes, over the course of 8 weeks (**Fig. S11A**). There was no significant difference in survival (**Fig. S11B**), or weight (**Fig. S11C**) between the recipients of the *Jag1$^{Ndr/Ndr}$* (n=6) and *Jag1$^{+/+}$* (n=8) lymphocytes. At the end of the 8th week, we sacrificed the mice and performed histological analysis of the intestine, scoring the intestinal inflammatory status [127]. There was no difference between the tested cohorts (**Fig. S11D, E**). Cumulatively, these data suggest there is no significant autoimmunity in the *Jag1$^{Ndr/Ndr}$* lymphocytic compartment.

Rag1$^{-/-}$ mice have previously been used to demonstrate the pro-fibrotic role of lymphocytes during cholestasis [44], making them a suitable model for testing the function of *Jag1 $^{Ndr/Ndr}$* lymphocytes in cholestasis. We thus further exploited the adaptive immune transfer to *Rag1$^{-/-}$* mice, testing the *Jag1^{Ndr}* lymphocyte contribution to fibrosis in the 3,5-diethoxycarbonyl-1,4-dihydrocollidine (DDC)-induced model of primary sclerosing cholangitis [128]. We harvested P30 donor *Jag1$^{+/+}$* or *Jag1$^{Ndr/Ndr}$* cells, transferred them into *Rag1$^{-/-}$* recipients, and four weeks later treated the mice with two weeks of DDC diet (**Fig. 5A**).

We analyzed the infiltration of Lck$^+$ T cells into the liver upon DDC-induced cholestasis using immunostaining on cryosections of the left lateral lobe (LLL), and by western blot analysis of the median lobe (ML). Both the *Jag1$^{+/+}$→Rag1$^{-/-}$* and *Jag1$^{Ndr/Ndr}$→Rag1$^{-/-}$* animals after DDC treatment had similar T cell infiltration in the LLL periportal areas, and in Lck levels in the ML (**Fig. 5B-C'**) suggesting no difference between *Jag1$^{Ndr/Ndr}$* and control T cells in the capacity of the control and mutant T cells to migrate into the liver upon injury.

To test the function of the transferred adaptive immune cells on fibrosis, we performed histological analysis on paraffin sections from the DDC-treated *Jag1$^{+/+}$→Rag1$^{-/-}$* and *Jag1$^{Ndr/Ndr}$→Rag1$^{-/-}$* LLL, assessing the collagen deposition with Sirius red staining. There was patent fibrosis both in the control and *Jag1$^{Ndr/Ndr}$* transduced *Rag1$^{-/-}$* mice (**Fig. 5D, D'**). To further discern if *Jag1$^{Ndr/Ndr}$* lymphocytes affect the composition of the fibrotic compartment, we stained the paraffin sections for cytokeratin 19 (CK19, a marker of cholangiocytes), alpha smooth muscle actin (aSMA myofibroblast and HSC marker), and Collagen 1a1 (COL1A1, an acute fibrotic marker expressed in response to liver injury by recently identified central vein-associated HSCs (CaHSC) [129]). Both aSMA, and COL1A1 levels and distribution were comparable between the *Jag1$^{Ndr/Ndr}$→Rag1$^{-/-}$* and *Jag1$^{+/+}$→Rag1$^{-/-}$* controls, following DDC treatment (**Fig. 5E**), indicating that *Jag1$^{Ndr/Ndr}$* T cells are either functionally equivalent to their WT counterpart or are not required for DDC-induced fibrosis.

Since patients with ALGS suffer from frequent infections [15], we next assessed the ability of the T cells to respond to bacterial infection in the recovery model of Dextran Sodium Sulphate (DSS) induced chronic ulcerative colitis, a well-established model of T cell response to bacterial infection [130,131]. Four weeks after the *Jag1$^{+/+}$→Rag1$^{-/-}$* and *Jag1$^{Ndr/Ndr}$→Rag1$^{-/-}$* lymphocyte transfer, mice were challenged with two consecutive 10 day-long 2.5% DSS diets, which induces bacterial infiltration of the intestinal submucosa and its inflammation, followed by 7 days of tissue recovery (**Fig. 5F**). Upon challenge, the *Rag1$^{-/-}$* recipients of the *Jag1$^{Ndr/Ndr}$* lymphocytes (n=5) manifested significantly lower frequencies of the CD44$^+$/CD4$^+$ and CD44$^+$/CD8$^+$ cells in the mesentery gland compared to *Jag1$^{+/+}$→ Rag1$^{/-}$* controls (n=4) (**Fig. 5G, G'**). This was in line with histological scoring of the intestinal and colon inflammatory status, which was significantly lower both in the intestine and colon of the *Jag1$^{Ndr/Ndr}$→Rag1$^{-/-}$* animals (**Fig. 5H, H'**).

In conclusion, the DDC experiments show that both the *Jag1$^{+/+}$* and *Jag1$^{Ndr/Ndr}$* lymphocytes can home to a cholestatic liver, while the lack of T-cell enrichment in *Jag1$^{Ndr/Ndr}$* livers at P10 (Fig 2F) indicate that a Jag1-compromised cholestatic liver, with delayed hepatocyte differentiation, does not attract T-cells. Importantly, the chronic ulcerative colitis model instead indicates either a developmental or intrinsic role for *Jag1* in CD4$^+$ and CD8$^+$ T cell activation in response to the bacterial infection, an intriguing phenotype well connected to the ALGS pathology [15,60].

DISCUSSION

Inflammation and fibrosis not only impair liver function and harm hepatocytes, but also initiate a cascade of events that can lead to liver cancer [132]. Liver disease evolution through stages of hepatic injury, inflammation, fibrosis, cirrhosis, and cancer are well understood[7,133], and fibrosis can in some cases be reversed, abrogating disease progression [134]. Degree of liver fibrosis can be scored according to METAVIR criteria ranging from F0 (no fibrosis) to F4 (Cirrhosis), but fibrosis can also be defined according to the region of the liver affected and the appearance of fibrosis. In cholestasis and biliary disease,

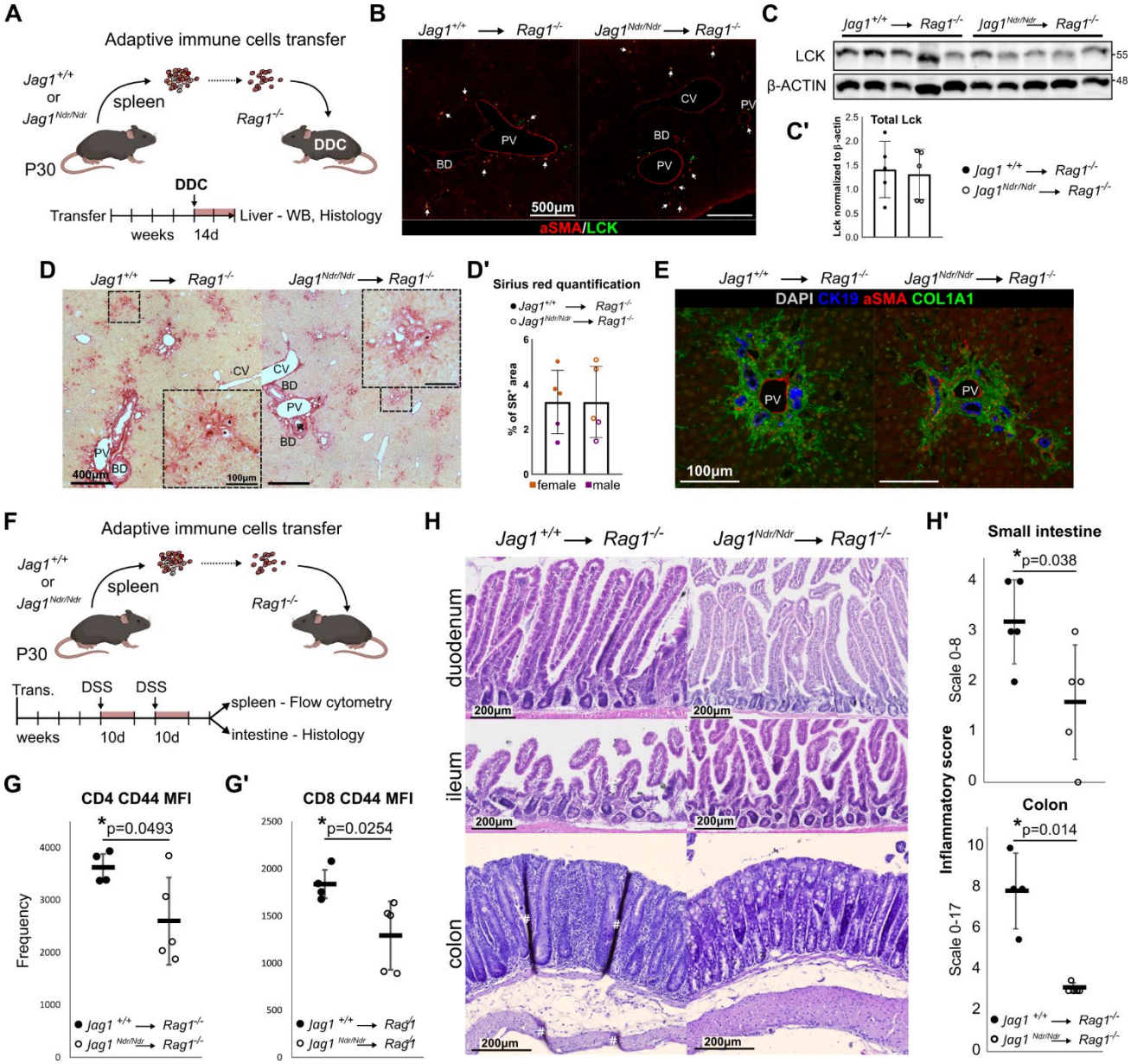

Figure 5: ***Jag1$^{Ndr/Ndr}$*** **lymphocytes are specifically deficient in mounting an inflammatory response to bacterial infection.** (**A**) Schematic of model for testing lymphocyte function in cholestasis. Lymphocytes are isolated from *Jag1$^{+/+}$* or *Jag1$^{Ndr/Ndr}$* spleens and transferred into *Rag1$^{-/-}$* mice. After 4 weeks, mice were fed a 3,5-diethoxycarbonyl-1,4-dihydrocollidine (DDC) diet for two weeks to induce cholestasis and fibrosis. After two weeks, mice were sacrificed for analysis. (**B**) Left lateral lobe (LLL) from *Jag1$^{+/+}$→Rag1$^{-/-}$* (left) and *Jag1$^{Ndr/Ndr}$→Rag1$^{-/-}$* (right) mice after DDC treatment, stained with antibodies against Lck and alpha-SMA. Arrows indicate DDC aggregates. (**C**) Western blot of Lck and β-actin levels in the liver median lobe lysate of the *Jag1$^{+/+}$→Rag1$^{-/-}$* and *Jag1$^{Ndr/Ndr}$→Rag1$^{-/-}$* after the DDC and respective quantification (C'). (**D, D'**) Representative image of paraffin sections from the left lateral lobe (LLL) of *Jag1$^{+/+}$→Rag1$^{-/-}$* (left) and *Jag1$^{Ndr/Ndr}$→Rag1$^{-/-}$* (right) mice after DDC treatment, stained with Sirius red (D), and corresponding quantification (D'). (**E, E'**) *Jag1$^{+/+}$→Rag1$^{-/-}$* and *Jag1$^{Ndr/Ndr}$→Rag1$^{-/-}$* mice after DDC diet stained with antibodies against CK19, alpha-SMA, and COL1A1 (E). (**F**) Schematic of the DSS-induced ulcerative colitis experimental model. Lymphocytes are isolated from *Jag1$^{+/+}$* or *Jag1$^{Ndr/Ndr}$* spleens and transferred into *Rag1$^{-/-}$* mice. Four weeks after lymphocyte transfer, mice are challenged with two consecutive 10 day-long 2.5% dextran sulfate sodium (DSS) diets, each followed by 7 days of tissue recovery. (**G, G'**) Quantification of flow cytometry analysis of the mesentery gland activated CD4^{+} and CD8^{+} T cell frequencies in *Jag1$^{+/+}$→Rag1$^{-/-}$* (n=4) and *Jag1$^{Ndr/Ndr}$→Rag1$^{-/-}$* mice (n=5 per genotype). (**H, H'**) Representative H&E sections of *Jag1$^{+/+}$→Rag1$^{-/-}$* or *Jag1$^{Ndr/Ndr}$→Rag1$^{-/-}$* duodenum, ileum and colon after DSS treatment (I), and the inflammatory score (I'). (mean ± SD, Statistical analysis was performed by unpaired, two-tailed Student's t-test, $p \leq 0.05$ = *). # - artefact; CV, central vein; PV, portal vein; BD, bile duct.

porto-portal and periportal fibrosis are common [135]. However, the genetic pediatric cholestatic disorder Alagille syndrome instead presents with pericellular or "chicken wire" fibrosis [43], which is instead characteristic of metabolic (dysfunction)-associated fatty liver disease or "MAFLD" (also known as non-alcoholic steatohepatitis (NASH)), and only rarely (in <1% of the cases) results in fibrosis, cirrhosis and HCC progression [36,37]. Another intriguing aspect of fibrosis is its reversibility, due to its transient nature challenging to "catch" in adults, but temporally defined in the pediatric cholangiopathies, better understanding is key to further treatment development[136].

We show here that *Jag1*$^{Ndr/Ndr}$ mice, in a mixed C3H/C53Bl6 background [61], are an ideal model for studying the function of Jag1 in ALGS in a genetic environment prone to spontaneous liver tumor formation. In this context, the H268Q mutation-carrying *Jag1*$^{Ndr/Ndr}$ mice are completely protected from HCC, displaying only mild fibrosis with distinct pericellular morphology, mimicking the fibrosis found in patients with ALGS [43]. This is a contrasting result to the pro-cancerogenic effect of disrupted Jag1/Notch2 signaling, recently reported in a diethylnitrosamine (DEN)-induced mouse model of HCC, in which inducible systemic deletion of Jag1 (by Mx1-cre or CreERT2) resulted in a higher number of tumors[34]. IN line with our results, in a hydrodynamic tail vein injection model of AKT-induced cholangiocarcinoma, Jag1 overexpression stimulated tumor formation, an effect that is preventable by concurrent overexpression of dominant-negative RBPJk [32]. Neither of these studies addressed the function of Jag1 on systems outside liver, which is relevant in the case of a systemic disease such as Alagille syndrome.

Interestingly, Tgf-β/SMAD signaling components (*Fos, Jun,* SMAD GSEA) were downregulated in *Jag1*$^{Ndr/Ndr}$ E16.5 hepatoblasts, while classic Notch targets were unaffected. However, silencing of both pathways in parallel would likely lead to complete inhibition of cholangiocyte differentiation, which is not observed in *Jag1* $^{Ndr/Ndr}$ mice, which do develop a biliary system with some delay [61]. Tgf-β signaling may be downregulated by the excess *Azgp1* in *Jag1* $^{Ndr/Ndr}$ animals. Azgp1 interacts with and negatively regulates both c/EBPα [151] and Tgf-β1-ERK2 signaling [152,153], and could thus hamper hepatoblast differentiation. The excess *Azgp1* itself could result from de-repression in the absence of Notch signaling, as NICD overexpression in prostate epithelium suppresses *Azgp1* expression [154]. However, exactly how *Azgp1* expression is regulated, and to what extent Azgp1 exerts a physiological function in hepatoblast differentiation remains to be elucidated. Interestingly, Tgf-β and Jag1-mediated Notch signaling act cooperatively, in a positive feedback loop that could be, in the presence of the mutated Jag1, disrupted by the presence of other Notch ligands such as Dll1 or Dll4 [18,155], also hampering hepatoblast specification into cholangiocytes.

We assessed to what extent the delayed differentiation of hepatocytes affects their ability to become activated upon cholestatic injury. Strikingly, neither E16.5 nor P3 mRNA scRNAseq expression profiles indicate upregulation of distress molecules or chemokines that are otherwise typically upregulated in primary hepatocyte activated by bile acids *in vitro* [81]. *Egr1* is an early stress response gene [156], that regulates hepatocyte clock genes [157], and its absence strongly attenuates inflammation in the BDL model of cholestasis [81]. The reduced expression of *Egr1* in E16.5 *Jag1*$^{Ndr/Ndr}$ hepatocytes is in line with its Notch activity-dependent decrease in hematopoietic stem cells in *Pofut1* KO mice [158]. *Egr1* may thus be Jag1/Notch signaling-responsive, and its downregulation in *Jag1*$^{Ndr/Ndr}$ hepatocytes may limit the capacity of hepatocytes to become activated and propagate the inflammatory response to cholestatic injury.

The reduced fibrosis, with chicken-wire appearance, in *Jag1*$^{Ndr/Ndr}$ mice recapitulates the fibrotic phenotype of patients with ALGS and shows that Jag1 is required for mounting a strong fibrotic response. Correspondingly, Notch activation in hepatocytes drives fibrosis in the context of MAFLD, and inhibition of Notch signaling attenuates MAFLD-associated fibrosis ([159] reviewed in [160]). Intriguingly, Notch signaling is not required for methionine-choline deficient (MCD) diet-induced fibrosis [159], demonstrating that fibrosis can be Notch-dependent or -independent, depending on the nature of the hepatic insult. Further resolving which cells must express Jag1 in order to develop robust fibrosis could thus be of interest both in ALGS and in MAFLD.

Limited hepatocyte activation could explain why neither NK or NKT cells populations, with pro and anti-fibrotic activity in neonatal stages [48,49,83], are affected in *Jag1*$^{Ndr/Ndr}$ animals. Similarly, in disagreement with the established role of T cells in fibrosis initiation and propagation (reviewed in [84,132]), there was no increase in T cell numbers in the *Jag1*$^{Ndr/Ndr}$ liver despite strong cholestasis. However, the strong reduction of the thymic size, made us reconsider the causality of phenotypic events. Thymus size can vary greatly in diseased conditions [161], but since the *Jag1*$^{Ndr/Ndr}$ thymus was small-for-size already at P0 (prior to cholestasis), it occurs in parallel to the liver phenotype. Interestingly, the splenomegaly in *Jag1*$^{Ndr/Ndr}$ mutants phenocopies the ALGS, in which it is attributed to portal hypertension [121], although splenomegaly has a higher prevalence than the hypertension [120]. These results suggest of a compensatory expansion of defective T cells, previously reported in immunodeficiencies such as Common Variable Immunodeficiency [122].

The thymic size reduction in *Jag1*$^{Ndr/Ndr}$ mice was not expected, although it is not entirely surprising, given the role of Notch in thymic development. The thymic stromal components that express Jag1 in both mouse and human are the vasculature, CD34^{+} mesenchymal cells [115,119], and mTECs, governing with DCs the elimination of autoreactive TCRαβ thymocytes [56,118]. Recent findings highlighted the role Notch1 signaling and Foxn1 in TECs differentiation [111,112,162], but neither the ligand nor the cell population expressing it were identified so far. There was no quantitative difference in TECs populations in *Jag1*$^{Ndr/Ndr}$ mutants at P30, suggesting that Jag1 signaling is not required for TEC differentiation and survival, but we cannot exclude a qualitative effect, resulting from the reduced signaling capacity of Jag1^{Ndr} ligand [61]. Apart for mTECs the hypomorphic Jag1 signaling-affected

populations could be the developing DCs [56,57], or thymocytes.

$CD4^+CD8^+$ DP cells are reduced in *Jag1*$^{Ndr/Ndr}$ thymi, and the αβ T cell lineage differentiation is skewed towards the $CD4^+$ - Treg lineage at the expense of $CD8^+$ cells. Tight control of Notch activation, achieved by correct combinatorial presence of different Notch ligands and receptors, is required for balanced development of the various T cell subtypes [113,163–166], reviewed in [54]. T cell differentiation from the hematopoietic progenitor cells starts only after Dll4/Notch1 activation occurs [165,167,168]. Further, the αβ T cell lineage development (giving rise to the conventional $CD4^+/CD8^+$ T cells) is dependent on Dll1/Notch1 signaling [118,163,169], while γδ T cell fate signal comes from Jag2 expressing cTECs [115] via Notch3 receptor on thymocytes [113].

Jag1 is less potent than Dll1 in inducing the DN1 into αβ T cell lineage, but more potent than Dll4 and Jag2, while Jag1 is more potent than Dll1, and less potent that Dll4 and Jag2 with regards to DN3 differentiation into γδ T cells [113,118]. While this does not explain the dysregulated DP progenitors, it is plausible that the lack of Jag1 intermediate-level activation from mTECs disturbed the maturation of the $CD4^+$ or $CD8^+$ SP progenitors after DP selection by providing a longer window to high-level activation by Dll1 (expressed both on cTECs and mTECs) [115]. Functionally, the lymphocyte transfer from control and *Jag1*$^{Ndr/Ndr}$ mutants to *Rag1*$^{-/-}$ mice suggest that the mTEC- and DC-facilitated selection of the SP T cells with autoreactive TCRs is not disrupted, ruling out the possibility of autoimmune phenotype.

$CD4^+$ SP differentiation into Tregs relies on Foxp3, the Notch target gene [170], and $CD4^+/CD25^+/Foxp3^+$ Tregs were enriched as a result of an off target Jag1 overexpression in a mouse NK1.1 transgene [171,172] or *in vitro* after co-culturing CD4+ T cells with Jag1-overexpressing DCs [173]. The proposed mechanisms likely involve a tissue-specific TCR-dependent activation via a Jag1-Notch1/Tgf-β axis [174,175] and TCR-independent co-activation of $CD4^+$ Notch3/OX40 receptors by Jag1-OX40L ligands [176,177]. These results are in contrast with the enriched Treg populations of the hypomorphic Jag1 signaling in *Jag1*$^{Ndr/Ndr}$ mice, however as our previous data suggest, the Jag1 missense mutation likely causes a selective impairment of the interaction with different Notch receptors [61], and deserves further experimental investigation.

Regardless of the underlying mechanism, the decreased numbers and maturation potential of the $CD8^+$ T cells as well as the observed higher frequency of Tregs are highly relevant from the perspective of cholestatic injury and fibrosis. While $CD8^+$ cytotoxic activity promotes liver fibrosis [178,179], Il2-expressing Tregs restrict biliary [47,180,181] and HCV-induced liver fibrosis [182], reviewed in [84]. Our experiments with DDC-induced sclerosing cholangitis did not reveal any difference in fibrosis in the presence of control ot *Jag1*$^{Ndr/Ndr}$ T cells. Strikingly, when challenged with the chronic bacterial infection, both *Jag1*$^{Ndr/Ndr}$ $CD4^+$ and $CD8^+$ T cells were less activated, suggesting that *Jag1*$^{Ndr/Ndr}$ T cells are not as potent inducers of inflammation as their WT counterparts. Fibrosis after DDC occurs through neutrophil-induced inflammation and Kupffer cell-mediated HSC activation[128,183] and thus might be independent of the T cell compartment. Other cholestatic models such as bile duct ligation (BDL), a surgically induced obstructive cholestasis, resulting in jaundice [70] with reported involvement of the $CD45^+$ cells [184,185] should therefore be tested to assess the impact of Jag1 abrogation on T cell-regulated fibrosis.

The bacteria-induced ulcerative colitis model results are also intriguing in the context of the ~ 25-35% of ALGS patients that suffer from recurring bacterial infections linked to an inability of $CD4^+$ cells to elicit the Th1 response [15,186] through a Jag1-mediated activation of CD46 receptor-expressing $CD4^+$ T cells [60,187]. As the recipient *Rag1*$^{-/-}$ mice are in a Bl6 background that dominantly employs a Th1 response after DSS-induced UC [188], we expect the lack of response in *Jag1*$^{Ndr/Ndr}$ animals to be at least partially due to disrupted Th1 response. So far it is unknown which cells provide the Jag1 signal required for the CD46 activation, but our data also suggest an intrinsic phenotype of the transferred cells as the recipient mice express WT Jag1 molecules. Thus, apart from the possibly disrupted clonal selection of T cells, reports of RBPJκ independent activity of Notch1 in $CD4^+$ T cells [189], co-regulated by a CD28 and cis-inhibiting Notch ligand crosstalk provide an alternative explanation [190], although clarifying the cis-inhibitory capacity of the mutant Jag1 calls for further research.

Nevertheless, the strength of our work is at factoring in multiple parallel phenotypes to assess the interaction of the immune system with the liver. In doing so we mapped a multi-layered mechanism in which Jag1 was required for differentiation of both hepatoblasts and adaptive immune cells, which may together modulate the fibrotic response to cholestasis. We also show that $CD4^+/CD8^+$ T cell dysregulation leads to immunodeficiency in a mouse model of ALGS, and may contribute to the antitumorigenic effects of JAG1 loss of function in ALGS. Thus, we believe our study expands our knowledge of ALGS pathology, liver fibrosis, HCC and Notch signaling in immune system development, and opens several new lines of research.

METHODS

Mouse maintenance and breeding

All animal experiments were performed in accordance with local rules and regulations and all experiments were approved by Stockholm's Norra Djurförsöksetiska nämnd (Stockholm animal research ethics board, ethics approval numbers: N50/14, N61/16, N5253/19, N2987/20) or Czech Academy of Sciences ethics board (approval number: AVCR 8362-2021). The *Jag1*$^{Ndr/Ndr}$ mice were maintained in a mixed C3H/C57bl6 genetic background as reported previously [61] and are deposited in the European Mouse Mutant Archive EMMA: https://www.infrafrontier.eu/search?keyword=EM:13207. *Rag1*-deficient animals were purchased from Jax (Jax: 002216). Animals were maintained with standard day/night cycles, provided with food and water ad libitum, and were housed in cages with enrichment. Males and females were

bred overnight and noon of day of plug was considered embryonic day (E) 0.5. Nodder mice were genotyped by the Transnetyx® (USA) automated qPCR genotyping company.

Adoptive T-cell transfer to Rag-deficient animals and Ulcerative colitis mouse model.

Adult Rag1-deficient animals (Jax: 002216) were used as the acceptors of T and B lymphocytes isolated from *Jag1*$^{+/+}$ or *Jag1*$^{Ndr/Ndr}$ mice. Spleens from *Jag1*$^{+/+}$ or *Jag1*$^{Ndr/Ndr}$ mice (littermates) were passed through 40 um nylon mesh to obtain a single cell suspension, which was then incubated overnight in 10% complete RPMI (Sigma-Aldrich, #R8758) to remove adherent cells. After the incubation, the floating fraction containing mainly lymphocytes was collected. One million lymphocytes were injected into the recipient via tail vein, in PBS. For the induction of colitis by DSS (Sigma-Aldrich, # D8906) mice were given 2.5% DSS in drinking water for one week, followed by 10 days of recovery and subsequently one more week of DSS treatment.

Mouse model of cholestasis

The DDC model of sclerosing cholestasis was induced by feeding a diet supplemented with 0.1% 3,5-diethoxycarbonyl-1,4-dihydrocollidine (DDC; Sniff, Soest, Germany) for 14 days. Mice were sacrificed after 14 days for analysis.

Immunohistochemistry and hematoxylin, and Sirius red staining

Table 1. Antibodies used in immunohistochemical or western blot analysis

Antigen	Clone		Dilution used	Company
anti-mouse-HRP	#ab205719	WB 1:20000	Abcam	
anti-rabbit-HRP	#ab205718	WB 1:20000	Abcam	
anti-β-actin	#sc-47778	WB 1:1000	Santa Cruz Biotechnology	
Lck	n.a.		h	Kind gift from Dominik Filipp
aSMA	M0851		IF 1:50	Dako
Collagen I	ab21286		IF 1:100	Abcam
CK19	TROMA-III RRID: AB_2133570		IF 1:250	DSHB

Liver section image acquisition

Mice > P10 were euthanized with CO2 or < P10 were decapitated, and liver was immediately dissected out, left lateral lobe was cut in half, one embedded in OCT and frozen on dry ice, and other fixed O/N in 4% PFA (VWR, #20909.290) in PBS, and processed for paraffine sectioning. Immunofluorescent staining was carried out on cryosections (14 µm) or paraffine sections (5 µm) as previously described [61,62]. The liver was imaged using the LSM 980 confocal microscope or SlideScanner (Carl Zeiss).

Western blotting

Mouse liver tissue was weighed and homogenized in RIPA Lysis and Extraction Buffer (Thermo Scientific, #89900) with the Protease and phosphatase inhibitor (Thermo Scientific, #A32961), using 15-25mg of tissue/200µl. Tissue samples were disrupted using a chilled glass-pestle homogenizer. Samples were then agitated for 2 hours at 4°C, and subsequently centrifuged at 16,000 rcf for 20 min at 4°C. The supernatant was collected, and the protein concentrations determined using the Pierce™ BCA Protein Assay Kit (Thermo Scientific, #23225). For western blotting, aliquots of 25 µg were denatured by boiling in Laemmli Sample Buffer (2x), separated by SDS-PAGE, and transferred onto PVDF membranes (Amersham™ Hybond®, # GE10600021) by electroblotting. The membrane was cut, blocked by 5% non-fat milk in 1X TBST (Tris-buffered saline, 0.1% Tween 20) for 1h/RT, and incubated ON/4°C with a Rabbit anti-Lck, and Mouse anti-β-actin antibodies. The following day, were membranes washed 4x/10min in 1X TBST and incubated with corresponding anti-rabbit-HRP or anti-mouse-HRP conjugated secondary antibodies for 1h/RT, followed by 4x/10min wash in 1X TBST. Chemiluminescence was detection with Pierce™ ECL Western Blotting Substrate (Thermo Fisher Scientific, #32209) on ChemiDoc machine (Bio-Rad).

Sample processing and flow cytometric analysis of embryo proper and yolk sac at E9.5

For dissociation and flow cytometry we followed a protocol described by Balounová and colleagues [196]. In brief, E9.5 embryo proper (EP) and yolk sac (YS) were dissected and dissociated separately. After briefly washing in cold Hank's balanced saline solution (HBSS) (Gibco, #14175095). EP and YS were incubated with 1 mg/mL Dispase (Gibco, #17105041) in HBSS for (~ 10 min for EP, ~17 min for YS) in 1.5mL Eppendorf tubes in water bath at 37°C, and occasionally mixed by gentle pipetting. The reaction was stopped by washing in HBSS with 2% FCS (Gibco, #10270106). Suspensions were passed through a 40µm cell

strainer (BD, #352350) and centrifuged at 350g/7min/4°C. Pelleted cells were resuspended in 200ul FACS wash (DPBS with 2% FBS, 2mM EDTA, Thermo Fisher, #AM9262) and transferred to 96-well V-bottom plates (Sigma-Aldrich, #BR781601) for further flow cytometric analysis. Primary antibody mixes (Table 2) were added and incubated for 30 min at 4°C, followed by LIVE/DEAD Fixable Aqua Dead Cell Stain (Thermo Fisher, # L34957) incubation for additional 30 min at 4°C. Cells were fixed for 15min/RT with fixation buffer from eBioscience™ FOXP3/ Transcription Factor Staining Buffer Set (eBioscience, #00-5523-00). Acquisition was performed on LSRII flow cytometer (BD Biosciences). All data were analysed using FlowJo software (FlowJo, V10.7.1).

Table 2. Antibodies used in E9.5 Flow cytometry

Antigen	Clone	Fluorophore	Laser line	BD LSRII	Dilution used	Company
CD41	MWReg30	BB515, FITC	Blue (488 nm)	525/50	100	Biolegend, #133903
CD117	ACK2	APC/eF660	Red (640nm)	670/14	50	Invitrogen, #17-1172-83
Viability dye	N/A	BV510	Violet (405 nm)	525/50	1000	Thermo Fisher
CD45	30-F11	Qdot585, BV570		585/42	100	Biolegend, #103135
TER119	TER-119	PE-Cy5.5	Yellow-Green (532nm)	710/50	100	Invitrogen, #35-5921-82
FcRγ	93	PE-Cy7		780/60	50	Biolegend, #101317

Single cell RNA seq and Flow cytometry: E16.5 and P3 sample preparation and sequencing

Reagents for the single-cell isolation: Tabletop centrifuge with cooling; QuadroMACS separator (Miltenyi, #130-091-051); Dead Cell Removal Kit (Miltenyi, #130-090-101); sterile 5ml Transfer Pipettes (Merc, #HS206371C-500EA); DPBS -Mg^{2+},-Ca^{2+} (Gibco, # D8537-500ML); HBSS -Mg^{2+},-Ca^{2+} (Gibco, #14175095); 2ml Eppendorf DNA LoBind® tubes (Merck, #EP0030108078), Liver digest medium (LDM) (Gibco; #17703034) - unfreeze in 4C, protect from light, avoid freeze-thaw; TrypLE Express (Gibco, 12604013); Millex-GV Filter 0.22 µm (Merck-Millipore, #SLGVR33RS); 40µm strainers (BD, #352350) or EASYstrainer (Greiner, #542040); 5ml FACS tubes with 70µm filter cap (Falcon, #38030); FCS (Gibco, #10270106); 0.5M EDTA pH 8.0 (Thermo Scientific, #R1021); BSA (Sigma-Aldrich, #A7906).

Buffers:

E16.5 - Wash Buffer (WB16-E) 1% BSA in HBSS, filter sterile (0.22 µm), Wash Buffer (WB16) 1% BSA, 1mM EDTA, HBSS, filter sterile (0.22 µm).

P3 - Wash Buffer (WBP3-E) 1% FCS in HBSS, filter sterile (0.22 µm), Wash Buffer (WBP3) 1% FCS, 1mM EDTA, HBSS, filter sterile (0.22 µm).

Embryo stage was determined based on the presence of vaginal plug, the morning after breeding initiation, noon of day of plug was considered as E0.5. All embryos at E16.5 and P3 pups from the *Jag1*$^{Ndr/+}$ x *Jag1*$^{Ndr/+}$ breeding were sacrificed by decapitation, their livers (and spleens at P3) dissected out and placed in 12- or 24-well plates with ice-cold DPBS on ice unless stated otherwise. In case of P3 pups we further determined the sex based on pigmentation of the scrotum [197].Material for genotyping was collected (tail or limb tissue) and processed for genotyping using TaqMan probe (Thermo Fisher) yielding results in 3 hours (P3 *Jag1*$^{Ndr/Ndr}$ pups were identified based on the presence of jaundice and random *Jag1*$^{Ndr/+}$ and *Jag1*$^{+/+}$ controls genotypes were confirmed afterwards). The tissue was kept in ice-cold DPBS for 30min before being transferred into 5ml FACS tubes with 1.5 ml LDM + 0.5 ml of TrypLE Express (E16.5) or 2ml LDM (P3 stage), pipetted 5x through sterile wide-bore blue tip (E16.5) or transfer pipettes (P3) and incubated at 37°C/5min in a water bath (inverting each tube after 2-3 minutes). After the 5 min incubation, we disrupted the tissue further by gentle pipetting of the tissue 10x using a filtered 1 ml tip, followed by an additional round of incubation at 37°C/5min in a water bath (inverting each tube after 2-3 minutes). The enzymatic digestion was terminated by addition of 1.5 ml of WB16-E/ WBP3-E and additional mechanical disruption of the remaining tissue by pipetting each sample 20x using filtered 1 ml wide-bore blue pipette tip. We immediately poured the suspension through 70 µm filters into FACS tubes, rinsed the filter once with 0.5 ml WB16/WBP3, and passed the filtered suspension through a 40 µm strainer, each sample into two 2 ml Eppi tubes.

The duplicates of E16.5/P3 samples were centrifuged at 100g for 5mins at 5°C. Each supernatant was transferred to two new tubes, while the pellets were resuspended in 200 µl of Dead Cell Removal MicroBead suspension in Binding buffer and the resuspended pellets were further incubated for 5min at RT. In the meantime, the supernatant from the

previous step was centrifuged at 250g for 5min at 5°C. The new supernatant was discarded, and the corresponding pellets were mixed with 200 µl of Dead Cell Removal MicroBeads with the previous cell suspension in Binding buffer. The mixture was incubated for 10min at RT. After the incubation 300 µl 1× Binding Buffer was added to the cell suspension to obtain a final volume of 500 µl, suitable for magnetic separation with MS columns. The separation was done based on the manufacturer's recommendations. Briefly, we rinsed the columns with 500 µl of 1× Binding Buffer, applied the cell suspension onto the column, and collected the flowthrough containing unlabeled cells (living cells). Columns were further washed three more times with 500µl of 1× Binding Buffer, flowthrough collected and 20 µl filter sterile 10% BSA was added to the purified cells. Resulting samples were divided in two, whereof 250 µl was used for scRNAseq, following the 10x Genomics® Single Cell Protocol, and the remainder was used for the flow cytometry as described below.

The duplicate P3 samples were centrifuged at 100g for 5min at 5°C, and supernatants were transferred to new tubes. The pelleted cells from each duplicate were pooled and resuspended in 1.5 ml of the WBP3-E buffer and transferred to a new 2 ml tube. In the meantime, the supernatants from the previous step were centrifuged at 250g for 5min at 5°C. The supernatants were discarded, and the corresponding pelleted cells were resuspended in 0.5 ml of the WBP3-E buffer and added to the resuspended cells obtained from the first centrifugation. The full sample cell suspensions (now in 2 ml of WBP3-E buffer) were then transferred into a new protein lo-bind tube through 40 µl cell strainer to remove any remaining cell debris or large clumps. We then determined the cell concentration using a Countess® II Quantification to calculate the appropriate volume for the subsequent resuspension to obtain the target concentrations of ~1200cells/µl as recommended by the 10x Genomics® Single Cell Protocol.

The whole procedure including tissue collection, genotyping and dissociation took 3 hours, before initiation of processing with 10x microfluidics chromium and/or for flow cytometry.

Flow cytometry E16.5, P3 - Staining

Single cell suspensions (cells) from liver and spleen were obtained as described above for single cell RNA-sequencing. Cells were washed twice and resuspended in FACS buffer (PBS with 2 mM EDTA and 2% FBS), filtered through a 100 µm strainer (BD Falcon) and stained in 96-well V-bottom plates. Unless otherwise stated, staining steps were performed with antibodies diluted according to the table X in 50 µl of the FACS buffer, at 4ºC in the dark, and washing steps were performed by resuspending the sample in 150 µl of the FACS buffer and centrifuging plates for 5 minutes at 500g at 4ºC. The BD Horizon Brilliant Stain Buffer Plus was added to the antibody mix in every step when the BD Horizon Brilliant dyes were used. Cells were pre-incubated with TruStain FcX (anti-CD16/32) to block Fc receptors for 10 minutes at room temperature. Cells were first stained with anti-CD64 antibody for 45 minutes. Next, cells were stained with antibodies against other surface antigens for 30 minutes, followed by two washes in FACS buffer. Cells were then stained with the LIVE/DEAD Fixable Aqua Dead Cell Stain (Thermo Fisher) and fluorescently conjugated streptavidin for 30 minutes. This was followed by two washes in FACS buffer. Next, cells were fixed for 45 minutes in 100 µl fixation/permeabilization working solution from eBioscience Foxp3/Transcription Factor Staining Buffer kit (Thermo Fisher) at room temperature. After this step, cells were washed in 1x permeabilization buffer from the same kit. Finally, cells were stained with antibodies against intracellular antigens diluted in 1x permeabilization buffer from the same kit for 30 minutes at room temperature. Samples were then washed twice in 1x permeabilization buffer and resuspended in FACS buffer for acquisition. For single-stained compensation controls, UltraComp eBeads Compensation Beads (Thermo Fisher) were used according to manufacturer's instructions. FACSymphony A5 flow cytometer (BD Biosciences) was used for acquisition. The instrument was equipped with the following lasers: UV (355 nm), violet (405 nm), blue (488 nm), yellow/green (561 nm) and red (637 nm). See Table 3 for details of the panel and cytometer configuration settings.

Table 3. Antibodies used in 25-color flow cytometry

Flow cytometry E16.5, P3 - Analysis

FCS3.0 files were exported from the FACSDiva and imported into FlowJo v.10.7.1 for analysis. The following plugin versions (from FlowJo Exchange) were used: FlowAI (2.1), DownSample (3.2), UMAP (3.1), PhenoGraph (3.0). The data were pre-processed using FlowAI (parameters selected: all checks, second fraction FR = 0.1, alpha FR = 0.01, maximum changepoints = 3, changepoint penalty = 500, dynamic range check side = both) to remove any anomalies present in FCS files. A compensation matrix was generated using AutoSpill in FlowJo. Events were downsampled from the live cell gate from all samples using DownSample, and categorical values were added to the downsampled populations (e.g., genotype, tissue) prior to concatenation so that groups of interest could be deconvoluted during the analysis. UMAP and PhenoGraph were run using all parameters from the panel except BV510. As over- and under-represented input groups are similarly weighted in the PhenoGraph output clusters, PhenoGraph results were normalized to account for the total number of cells from each input group. Some figures were generated in RStudio (version 1.3.959) using RColorBrewer (v1.1-2), ggplot2 (v3.2.1 and v3.3.0), tidyr (v.1.0.2), reshape2 (v.1.4.3), and pheatmap (v.10.12).

Antigen	Clone	Fluorophore	Laser line	BD FACSymphony filter	Dilution used	Company
CD45	30-F11	BUV395	UV (355 nm)	379/28	100	BD Biosciences
CD31	390	BUV496		515/30	100	BD Biosciences
CD49a	Ha31/8	BUV563		580/20	400	BD Biosciences
TCR-beta	H57-597	BUV615		605/20	100	BD Biosciences
TER119	TER-119	BUV661		670/25	200	BD Biosciences
CD11b	M1/70	BUV737		735/30	200	BD Biosciences
EpCAM	G8.8	BUV805		810/40	100	BD Biosciences
Ly6C	AL-21	FITC	Blue (488 nm)	530/30	200	BD Biosciences
CD34	MEC14.7	Biotin		N/A	50	Biolegend
Streptavidin	NA	BB630		610/20	400	BD Biosciences
Tim-4	RMT4-54	BB700		710/50	100	BD Biosciences
Jag1	HMJ1-29	APC	Red (637 nm)	670/30	100	Biolegend
CD3	17A2	AF700		730/45	200	Biolegend
MHC-II	I-A/I-E	APC-Fire750		780/60	400	Biolegend
CD117	2B8	BV421	Violet (405 nm)	450/50	50	Biolegend
Viability dye	NA	BV510		525/50	100	Thermo Fisher
CD4	RM4-5	BV570		586/15	400	Biolegend
Ly6G	1A8	BV605		605/40	200	BD Biosciences
CD19	6D5	BV650		677/20	200	Biolegend
Siglec-F	E50-2440	BV711		710/50	200	BD Biosciences
CD71	C2	BV750		750/30	100	BD Biosciences
CD64	X54-5/71	BV786		810/40	100	BD Biosciences
Nestin	307501	PE	Yellow-Green (561 nm)	586/15	400	Thermo Fisher
NKp46	29A1.4	PE-Dazzle 594		610/20	50	Biolegend
F4/80	BM8	PE-Cy5		670/30	100	Biolegend
CD8	53-6.7	PE-Cy5.5		710/50	400	Thermo Fisher
CD11c	N418	PE-Cy7		780/60	200	Biolegend
TruStain FcX (CD16/32)	93	NA	NA	NA	100	Biolegend
Brilliant Stain Buffer Plus	N/A	N/A	N/A	N/A	5	BD Biosciences

Flow cytometry analysis of thymic epithelial cells

Thymi from 4-week-old *Jag1*$^{+/+}$ or *Jag1*$^{Ndr/Ndr}$ mice were minced by scissors into small pieces and dissociated by enzymatic digestion for 30min at 37 °C using 0.3 mg ml−1 collagenase D (Roche), 1 mg ml−1 dispase II (Gibco) and 10 ng ml−1 DNase I (Sigma-Aldrich) in RPMI supplemented with 2% FBS. Percoll density gradient

centrifugation was performed to enrich for thymic epithelial cells. Cells were resuspended in 2 ml of 1.115 g ml−1 isotonic Percoll (Sigma-Aldrich) and placed at the bottom of a tube. Subsequently, 1 ml of isotonic 1.065 g ml−1 Percoll and then 1 ml of PBS were layered on top. The Percoll gradient was run at 2,700 rpm (1451xg), at 4 °C, with no acceleration or brake for 30 min in the Eppendorf 5804 R centrifuge with S–4–72 rotor. The thymic epithelial cells were collected and subjected to flow cytometric analysis using the following set of antibodies for extracellular staining: CD45 APC-Cy7, EpCAM, APC, Ly6d PB, MHCII PE (all Biolegend). Intracellular staining of Aire AF488 (Invitrogen) was done after fixation and permeabilization of cells by the Foxp3/Transcription factor fixation buffer set (Thermo) according to manufacturer's instructions. Extracellular cell staining for flow cytometry analysis was performed at 4°C, in the dark, on ice, for 30 minutes, while the fixation and intracellular staining was performed at room temperature, in the dark for 40 minutes (each step). Dead cells were excluded by addition of Viability dye 506 (Thermo) prior to fixation. Samples were analysed using a BD LSRII flow cytometer and FlowJO software version 10.7 (BD).

Flow cytometry analysis of the T-cell compartment

Spleens and thymi of *Jag1*$^{+/+}$ or *Jag1*$^{Ndr/Ndr}$ mice were passed through 40 um nylon mesh to obtain a single cell suspension. The following antibodies were used for T-cell analysis: CD4 BV785, CD44 BV 711, CD8 Percp-Cy5.5, TCR-B APC-Cy7 (all Biolegend). Extracellular cell staining for flow cytometry analysis was performed at 4°C, in the dark, on ice, for 30 min. Dead cells were excluded from analysis by addition of Viability dye 506 (Thermo) prior to the fixation. The fixation was performed at room-temperature in dark for 40 minutes using Foxp3/Transcription factor fixation buffer set (Thermo). Foxp3 BV421 (BD) staining was done at room temperature in dark for 40 minutes. Samples were analysed using BD LSRII flow cytometer and FlowJO software version 10.7 (BD).

Library preparation and sequencing

The E16.5, P3 samples were processed on a Chromium microfluidics platform (10X Genomics) using the Chromium™ Single Cell 3' Library and Gel Bead Kit v2 (10X Genomics, # PN-120237) and the Chromium™ Single Cell A Chip Kit (10X Genomics, #PN-120236) following the manufacturer's instructions. The E16.5 library preparation, validation with Bioanalyzer High Sensitivity DNA kit (Agilent, # 5067-4626), and sequencing with NovaSeq (100 cycles) platform was performed by the SciLifeLab, Stockholm. The P3 samples, library preparation, validation with Bioanalyzer High Sensitivity DNA kit (Agilent, # 5067-4626), and sequencing with NextSeq550 (75 cycles) or S4 Novaseq platform was performed by the Bioinformatics and Expression analysis core facility (BEA), Huddinge, Stockholm.

Analysis of the scRNA seq using Seurat packages

Demultiplexing, quality control, raw data, gene expression data counts were performed using CellRanger (Chromium), by the BEA and SciLife core facilities. Matrices were further processed and analyzed with R (version 4.1.2) in R Studio. Prior to transformation into Seurat Objects, matrices were precleared using SoupX [198] with default settings of setContaminationFraction parameter (sc) for the P3, and (sc, 0.13) for the E16.5 stages. All bioinformatic analyses was performed using Seurat pipeline, doublet removal with scDblFinder [199], QC cutoffs for E16.5 datasets were nFeature_RNA > 500 & nFeature_RNA < 7000 & percent.mt < 10, for P3 a range of nFeature_RNA > 300-500 & nFeature_RNA < 4500-6000 & percent.mt < 10 were used, followed by SCT based integration of the E16.5 and P3 *Jag1*$^{+/+}$, *Jag1*$^{Ndr/+}$, and *Jag1*$^{Ndr/Ndr}$ datasets [71]. In total, 183,542 cells passed through the cross-contamination adjustment, quality control filtering and doublet removal in each of the duplicates per genotype and stage, analyzed in Seurat [71] (**Fig. 2B, B'**). A mean of 1520 genes, 6703 reads, and 3.0% of mitochondrial mRNA content were detected per cell. For comparative transcriptomic analysis, logNorm and scaled RNA data were used. The GSEA was performed using clusterProfiler [98], and pseudotime analysis was with monocle3 [93] packages.

Deconvolution of bulk RNA seq using MuSIC packages

To estimate changes in cell type proportions in *Jag1*$^{Ndr/Ndr}$ livers compared to *Jag1*$^{+/+}$ livers at P10, we used our previously generated bulk RNA-seq datasets (GSE104875) [61]. We employed a method for cell type deconvolution of bulk tissue RNA-seq with multi-subject single-cell expression reference called MuSiC [109]. As a reference single cell RNA-seq dataset, we chose an annotated dataset by Liang and colleagues, available as a filtered feature matrix under GEO accession number GSE171993 [4]. We imported the dataset to R 4.1.0 package Seurat 4.0.5 [200] and used the subset of the data corresponding to P1, P3 and P7. The original annotation accounted for 30 cell types in liver scRNA-seq data [4]. We filtered for high-quality cells containing < 5% of mitochondrial genes expressed per cell and 200 - 4000 genes per cell, and for genes that are expressed in at least 3 cells, resulting in a dataset of 32,967 cells and 23,170 genes. The Seurat object was converted to an Expression set, required as input in MuSiC using a function SeuratToExpressionSet from BisqueRNA 1.0.5 R package [201]. The MuSiC was performed using music_prop function. To analyze the differentiation signature of hepatocytes, we further subset neonatal hepatocytes (P1, P3, P7) from scRNA-seq dataset (1281 cells), converted to Expression set and used this as a scRNA-seq reference for MuSiC on the P10 bulk RNA-seq dataset.

ACKNOWLEDGEMENTS: The data handling and initial computations were enabled by resources in projects [SNIC 2018/8-200 and SNIC 2020-16-189] provided by the Swedish National Infrastructure for Computing (SNIC) at UPPMAX, partially funded by the Swedish Research Council through grant agreement no. 2018-05973. We thank the core facility at Novum, BEA, Bioinformatics and

Expression Analysis, which is supported by the board of research at the Karolinska Institute and the research committee at the Karolinska hospital. We thank Raoul Kuiper and the FENO core facility for immunohistochemical staining of JAG1 in adult mice, and for discussions. We thank Stefaan Verhulst for fruitful discussions of HSC biology and analyses which are not included in this version of the manuscript. We thank Katarina Kováčová for excellent technical support, Sandra De Haan for assistance with collection of biological material, and Roman Hillje for his easy-to-use templates for visualization in R https://roman-haa.github.io/projects/scrnaseq_workflow/. This work was supported by the following grant agencies: Wenner-Gren Foundation, The European Association for the Study of the Liver (EASL: The Daniel Alagille Award to ERA and the Sheila Sherlock Post Doc fellowship to JM), funding from Karolinska Institutet (2-560/2015-280, 2-2110/2019-7, 2-195/2021), KI/SLL Center for Innovative Medicine (CIMED, 2-538/2014-29), Alex & Eva Wallström Foundation, and PRIMUS/21/SCI/006 project, funded by Charles University Grant Agency to J.M.

How each author was involved with the manuscript (e.g., [1]study concept and design; [2]acquisition of data; [3]analysis and interpretation of data; [4]drafting of the manuscript; [5]critical revision of the manuscript for important intellectual content; [6]statistical analysis; [7]obtained funding; [8]technical, or material support; [9]study supervision) [123456789]

JM[12345679], **IF**[12356], **SH**[23568], **JH**[2356], **NVH**[2358], **LB**[365], **MJ**[236], **AMF**[23], **FT**[23], **DVO**[23], **IČ**[36], **LS**[28], **EV**[28], **TB**[8], **NB**[13789], **MG**[3789], **JD**[1379], **ERA**[12345679]

REFERNCES:

1. Gordillo M, Evans T, Gouon-Evans V. Orchestrating liver development. Development [Internet]. 2015 [cited 2015 Jul 5];142:2094–108. Available from: http://www.ncbi.nlm.nih.gov/pubmed/26081571

2. Nakagaki BN, Mafra K, de Carvalho É, Lopes MAFMEMAF, Carvalho-Gontijo R, de Castro-Oliveira HM, et al. Immune and metabolic shifts during neonatal development reprogram liver identity and function. J Hepatol [Internet]. Elsevier; 2018 [cited 2019 Nov 15];69:1294–307. Available from: https://www.sciencedirect.com/science/article/abs/pii/S0168827818323018

3. Soares-da-Silva F, Peixoto M, Cumano A, Pinto-do-Ó P. Crosstalk Between the Hepatic and Hematopoietic Systems During Embryonic Development [Internet]. Front. Cell Dev. Biol. Frontiers Media S.A.; 2020 [cited 2020 Aug 22]. Available from: /pmc/articles/PMC7387668/?report=abstract

4. Liang Y, Kaneko K, Xin B, Lee J, Sun X, Zhang K, et al. Temporal analyses of postnatal liver development and maturation by single-cell transcriptomics. Dev Cell [Internet]. Cell Press; 2022 [cited 2022 Feb 21];57:398-414.e5. Available from: https://linkinghub.elsevier.com/retrieve/pii/S1534580722000041

5. Fabris L, Fiorotto R, Spirli C, Cadamuro M, Mariotti V, Perugorria MJ, et al. Pathobiology of inherited biliary diseases: a roadmap to understand acquired liver diseases. Nat. Rev. Gastroenterol. Hepatol. Nature Publishing Group; 2019. p. 497–511.

6. Van Hul N, Lendahl U, Andersson ER. Mouse Models for Diseases in the Cholangiocyte Lineage. Humana Press, New York, NY; 2019 [cited 2019 Nov 18]. p. 203–36. Available from: http://link.springer.com/10.1007/978-1-4939-9420-5_14

7. Llovet JM, Kelley RK, Villanueva A, Singal AG, Pikarsky E, Roayaie S, et al. Hepatocellular carcinoma. Nat Rev Dis Prim 2021 71 [Internet]. Nature Publishing Group; 2021 [cited 2022 Aug 24];7:1–28. Available from: https://www.nature.com/articles/s41572-020-00240-3

8. Mašek J, Andersson ER. The developmental biology of genetic Notch disorders. Development [Internet]. 2017;144:1743–63. Available from: http://www.ncbi.nlm.nih.gov/pubmed/28512196

9. Siebel C, Lendahl U. Notch signaling in development, tissue homeostasis, and disease. Physiol Rev [Internet]. American Physiological Society; 2017 [cited 2017 Nov 16];97:1235–94. Available from: http://physrev.physiology.org/lookup/doi/10.1152/physrev.00005.2017

10. Oda T, Elkahloun AG, Pike BL, Okajima K, Krantz ID, Genin A, et al. Mutations in the human Jagged1 gene are responsible for Alagille syndrome. Nat Genet [Internet]. Nature Publishing Group; 1997 [cited 2013 Sep 4];16:235–42. Available from: http://www.nature.com/doifinder/10.1038/ng0797-235

11. Li L, Krantz ID, Deng Y, Genin A, Banta AB, Collins CC, et al. Alagille syndrome is caused by mutations in human Jagged1, which encodes a ligand for Notch1. Nat Genet [Internet]. Nature Publishing Group; 1997 [cited 2016 Jul 7];16:243-51. Available from: http://www.nature.com/doifinder/10.1038/ng0797-243

12. Gilbert MA, Bauer RC, Rajagopalan R, Grochowski CM, Chao G, McEldrew D, et al. Alagille syndrome mutation update: Comprehensive overview of JAG1 and NOTCH2 mutation frequencies and insight into missense variant classification. Hum Mutat [Internet]. John Wiley and Sons Inc.; 2019 [cited 2020 May 2];40:2197–220. Available from: https://onlinelibrary.wiley.com/doi/abs/10.1002/humu.23879

13. McDaniell R, Warthen DM, Sanchez-Lara PA, Pai A, Krantz ID, Piccoli DA, et al. NOTCH2 mutations cause Alagille syndrome, a heterogeneous disorder of the notch signaling pathway. Am J Hum Genet [Internet]. 2006 [cited 2013 Sep 4];79:169–73. Available from: http://www.ncbi.nlm.nih.gov/pubmed/16773578

14. Alagille D, Odièvre M, Gautier M, Dommergues JPP. Hepatic ductular hypoplasia associated with characteristic facies, vertebral malformations, retarded physical, mental, and sexual development, and cardiac murmur. J Pediatr [Internet]. 1975 [cited 2014 Feb 4];86:63–71. Available from: http://www.ncbi.nlm.nih.gov/pubmed/803282

15. Tilib Shamoun S, Le Friec G, Spinner N, Kemper C, Baker AJ. Immune dysregulation in Alagille syndrome: A new feature of the evolving phenotype. Clin Res Hepatol Gastroenterol [Internet]. Elsevier Masson; 2015 [cited 2019 Nov 17];39:566–9. Available from: https://www.sciencedirect.com/science/article/pii/S2210740115000418

16. Hofmann JJ, Zovein AC, Koh H, Radtke F, Weinmaster G, Iruela-Arispe ML, et al. Jagged1 in the portal vein mesenchyme regulates intrahepatic bile duct development: insights into Alagille syndrome. Development [Internet]. Oxford University Press for The Company of Biologists Limited; 2010 [cited 2014 Feb 11];137:4061–72. Available from: http://www.ncbi.nlm.nih.gov/pubmed/21062863

17. Zong Y, Panikkar A, Xu J, Antoniou A, Raynaud P, Lemaigre F, et al. Notch signaling controls liver development by regulating biliary differentiation. Development [Internet]. The Company of Biologists Ltd; 2009 [cited 2015 Aug 20];136:1727–39. Available from: http://www.ncbi.nlm.nih.gov/pubmed/19369401

18. Kaylan KB, Ermilova V, Yada RC, Underhill GH. Combinatorial microenvironmental regulation of liver progenitor differentiation by Notch ligands, TGFβ, and extracellular matrix. Sci Rep [Internet]. Nature Publishing Group; 2016 [cited 2020 Jul 28];6:1–15. Available from: www.nature.com/scientificreports

19. Yang L, Wang WH, Qiu WL, Guo Z, Bi E, Xu CR. A single-cell transcriptomic analysis reveals precise pathways and regulatory mechanisms underlying hepatoblast differentiation. Hepatology [Internet]. John Wiley and Sons Inc.; 2017 [cited 2021 Jun 15];66:1387–401. Available from: https://aasldpubs.onlinelibrary.wiley.com/doi/full/10.1002/hep.29353

20. Kodama Y, Hijikata M, Kageyama R, Shimotohno K, Chiba T. The role of notch signaling in the development of intrahepatic bile ducts. Gastroenterology [Internet]. Elsevier; 2004 [cited 2016 Nov 21];127:1775–86. Available from: http://linkinghub.elsevier.com/retrieve/pii/S0016508504015732

21. Han H, Tanigaki K, Yamamoto N, Kuroda K, Yoshimoto M, Nakahata T, et al. Inducible gene knockout of transcription factor recombination signal binding protein-J reveals its essential role in T versus B lineage decision. Int Immunol [Internet]. Oxford University Press; 2002 [cited 2016 Nov 9];14:637–45. Available from: http://www.ncbi.nlm.nih.gov/pubmed/12039915

22. Herman BC, Jenkinson WE, Parnell SM, Rossi SW, Jenkinson EJ, Anderson G. T/B lineage choice occurs prior to intrathymic Notch signaling. Blood [Internet]. American Society of Hematology; 2005 [cited 2022 Jun 4];106:886–92. Available from: https://ashpublications.org/blood/article/106/3/886/21869/T-B-lineage-choice-occurs-prior-to-intrathymic

23. Kumano K, Chiba S, Kunisato A, Sata M, Saito T, Nakagami-Yamaguchi E, et al. Notch1 but not Notch2 is essential for generating hematopoietic stem cells from endothelial cells. Immunity. Cell Press; 2003;18:699–711.

24. Laruy B, Garcia-Gonzalez I, Casquero-Garcia V, Benedito R. Endothelial-to-hematopoietic transition is induced by Notch glycosylation and upregulation of Mycn. bioRxiv [Internet]. Cold Spring Harbor Laboratory; 2020 [cited 2020 Oct 20];2020.09.13.295238. Available from: https://doi.org/10.1101/2020.09.13.295238

25. Robert-Moreno À, Guiu J, Ruiz-Herguido C, López ME, Inglés-Esteve J, Riera L, et al. Impaired embryonic haematopoiesis yet normal arterial development in the absence of the Notch ligand Jagged1. EMBO J [Internet]. John Wiley & Sons, Ltd; 2008 [cited 2020 Jul 28];27:1886–95. Available from: http://emboj.embopress.org/cgi/doi/10.1038/emboj.2008.113

26. Chen ELY, Thompson PK, Zúñiga-Pflücker JC. RBPJ-dependent Notch signaling initiates the T cell program in a subset of thymus-seeding progenitors. Nat Immunol [Internet]. Nature Publishing Group; 2019 [cited 2020 Nov 29];20:1456–68. Available from: https://pubmed.ncbi.nlm.nih.gov/31636466/

27. Villanueva A, Alsinet C, Yanger K, Hoshida Y, Zong Y, Toffanin S, et al. Notch signaling is activated in human hepatocellular carcinoma and induces tumor formation in mice. Gastroenterology [Internet]. Elsevier; 2012 [cited 2013 Sep 4];143:1660-1669.e7. Available from: http://www.ncbi.nlm.nih.gov/pubmed/22974708

28. Jin Y, Li C, Xu D, Zhu J, Wei S, Zhong A, et al. Jagged1-mediated myeloid Notch1 signaling activates HSF1/Snail and controls NLRP3 inflammasome activation in liver inflammatory injury. Cell Mol Immunol [Internet]. Chinese Soc Immunology; 2019 [cited 2020 Jul 28];1–12. Available from: https://doi.org/10.1038/s41423-019-0318-x

29. Xie G, Karaca G, Swiderska-Syn M, Michelotti GA, Krüger L, Chen Y, et al. Cross-talk between Notch and Hedgehog regulates hepatic stellate cell fate in mice. Hepatology [Internet]. John Wiley & Sons, Ltd; 2013 [cited 2020 Feb 29];58:1801–13. Available from: http://doi.wiley.com/10.1002/hep.26511

30. Huang M, Chang A, Choi M, Zhou D, Anania FA, Shin CH. Antagonistic interaction between Wnt and Notch activity modulates the regenerative capacity of a zebrafish fibrotic liver model. Hepatology [Internet]. 2014 [cited 2016 Oct 5];60:1753–66. Available from: http://www.ncbi.nlm.nih.gov/pubmed/24995814

31. Gao J, Chen C, Hong L, Wang J, Du Y, Song J, et al. Expression of Jagged1 and its association with hepatitis B virus X protein in hepatocellular carcinoma. Biochem Biophys Res Commun [Internet]. 2007 [cited 2013 Dec 3];356:341–7. Available from: http://www.ncbi.nlm.nih.gov/pubmed/17359939

32. Che L, Fan B, Pilo MG, Xu Z, Liu Y, Cigliano A, et al. Jagged 1 is a major Notch ligand along cholangiocarcinoma development in mice and humans. Oncogenesis [Internet]. Nature Publishing Group; 2016 [cited 2022 Sep 20];5:e274. Available from: /pmc/articles/PMC5177771/

33. Wang M, Xue L, Cao Q, Lin Y, Ding Y, Yang P, et al. Expression of Notch1, Jagged1 and beta-catenin and their clinicopathological significance in hepatocellular carcinoma. Neoplasma [Internet]. 2009 [cited 2013 Dec 3];56:533–41. Available from: http://www.ncbi.nlm.nih.gov/pubmed/19728763

34. Nakano Y, Nakao S, Sueoka M, Kasahara D, Tanno Y, Sumiyoshi H, et al. Two distinct Notch signals, Delta-like 4/Notch1 and Jagged-1/Notch2, antagonistically regulate chemical hepatocarcinogenesis in mice. Commun Biol [Internet]. Nature Publishing Group; 2022 [cited 2022 Feb 4];5:1–10. Available from: https://www.nature.com/articles/s42003-022-03013-8

35. Kim E-J, Kim JY, Kim S-O, Ham SW, Choi S-H, Hong N, et al. JAG1 intracellular domain acts as a transcriptional cofactor that forms an oncogenic transcriptional complex with DDX17/SMAD3/TGIF2. bioRxiv [Internet]. Cold Spring Harbor Laboratory; 2021 [cited 2021 Nov 1];2021.03.31.437839. Available from: https://www.biorxiv.org/content/10.1101/2021.03.31.437839v3

36. Schindler EA, Gilbert MA, Piccoli DA, Spinner NB, Krantz ID, Loomes KM. Alagille syndrome and risk for hepatocellular carcinoma: Need for increased surveillance in adults with mild liver phenotypes. Am J Med Genet Part A [Internet]. John Wiley & Sons, Ltd; 2021 [cited 2021 Dec 16];185:719–31. Available from: https://onlinelibrary.wiley.com/doi/full/10.1002/ajmg.a.62028

37. Vandriel SM, Li L, She H, Wang J, Gilbert MA, Jankowska I, et al. Natural History of Liver Disease in a Large International Cohort of Children with Alagille syndrome: Results from The GALA Study. Hepatology [Internet]. Hepatology; 2022 [cited 2022 Sep 23]; Available from: https://pubmed.ncbi.nlm.nih.gov/36036223/

38. Hadžić N, Quaglia A, Portmann B, Paramalingam S, Heaton ND, Rela M, et al. Hepatocellular carcinoma in biliary atresia: King's College Hospital experience. J Pediatr. 2011;159:617-22.e1.

39. Knisely AS, Strautnieks SS, Meier Y, Stieger B, Byrne JA, Portmann BC, et al. Hepatocellular carcinoma in ten children under five years of age with bile salt export pump deficiency. Hepatology [Internet]. 2006 [cited 2013 Dec 3];44:478–86. Available from: http://www.ncbi.nlm.nih.gov/pubmed/16871584

40. Strautnieks SS, Byrne JA, Pawlikowska L, Cebecauerová D, Rayner A, Dutton L, et al. Severe Bile Salt Export Pump Deficiency: 82 Different ABCB11 Mutations in 109 Families. Gastroenterology [Internet]. 2008 [cited 2013 Dec 6];134:1203–14. Available from: http://www.ncbi.nlm.nih.gov/pubmed/18395098

41. Schady DA, Roy A, Finegold MJ. Liver tumors in children with metabolic disorders. Transl Pediatr [Internet]. AME Publications; 2015 [cited 2022 Sep 5];4:290. Available from: /pmc/articles/PMC4728996/

42. Schoen K, Ribeiro CM de F, Gonçalves MC, de Souza ARM, Porta G, Horvat N. Hepatocellular carcinoma in an adult with Alagille syndrome: case report and literature review. Radiol Case Reports. Elsevier; 2021;16:90–3.

43. Fabris L, Cadamuro M, Guido M, Spirli C, Fiorotto R, Colledan M, et al. Analysis of liver repair mechanisms in Alagille syndrome and biliary atresia reveals a role for notch signaling. Am J Pathol [Internet]. American Society for Investigative Pathology; 2007 [cited 2019 Jan 21];171:641–53. Available from: http://www.ncbi.nlm.nih.gov/pubmed/17600123

44. Joshi N, Kopec AK, Cline-Fedewa H, Luyendyk JP. Lymphocytes contribute to biliary injury and fibrosis in experimental xenobiotic-induced cholestasis. Toxicology. Elsevier; 2017;377:73–80.

45. Shinkai M, Shinkai T, Puri P, Stringer MD. Elevated expression of IL2 is associated with increased infiltration of CD8+ T cells in biliary atresia. J Pediatr Surg [Internet]. J Pediatr Surg; 2006 [cited 2021 Jun 27]. p. 300–5. Available from: https://pubmed.ncbi.nlm.nih.gov/16481239/

46. Shivakumar P, Sabla G, Mohanty S, McNeal M, Ward R, Stringer K, et al. Effector Role of Neonatal Hepatic CD8+ Lymphocytes in Epithelial Injury and Autoimmunity in Experimental Biliary Atresia. Gastroenterology [Internet]. W.B. Saunders; 2007 [cited 2021 Jun 27];133:268–77. Available from: https://pubmed.ncbi.nlm.nih.gov/17631148/

47. Katz SC, Ryan K, Ahmed N, Plitas G, Chaudhry UI, Kingham TP, et al. Obstructive Jaundice Expands Intrahepatic Regulatory T Cells, Which Impair Liver T Lymphocyte Function but Modulate Liver Cholestasis and Fibrosis. J Immunol [Internet]. American Association of Immunologists; 2011 [cited 2021 Nov 4];187:1150–6. Available from: https://www.jimmunol.org/content/187/3/1150

48. Shivakumar P, Sabla GE, Whitington P, Chougnet CA, Bezerra JA. Neonatal NK cells target the mouse duct epithelium via Nkg2d and drive tissue-specific injury in experimental biliary atresia. J Clin Invest [Internet]. American Society for Clinical Investigation; 2009 [cited 2022 Mar 4];119:2281–90. Available from: http://www.jci.org

49. Squires JE, Shivakumar P, Mourya R, Bessho K, Walters S, Bezerra JA. Natural killer cells promote long-term hepatobiliary inflammation in a low-dose rotavirus model of experimental biliary atresia. PLoS One [Internet]. Public Library of Science; 2015 [cited 2021 Mar 23];10. Available from: https://pubmed.ncbi.nlm.nih.gov/25992581/

50. Duwaerts CC, Sun EP, Cheng CW, Van Rooijen N, Gregory SH. Cross-activating invariant NKT cells and Kupffer cells suppress cholestatic liver injury in a mouse model of biliary obstruction. PLoS One [Internet]. PLoS One; 2013 [cited 2021 Jun 27];8. Available from: https://pubmed.ncbi.nlm.nih.gov/24260285/

51. P W, CW C, S G, BL H, M H, L B, et al. Invariant natural killer T cells suppress the neutrophil inflammatory response in a mouse model of cholestatic liver damage. Gastroenterology [Internet]. Gastroenterology; 2009 [cited 2021 Nov 4];136. Available from: https://pubmed.ncbi.nlm.nih.gov/19056387/

52. Cai SY, Ge M, Mennone A, Hoque R, Ouyang X, Boyer JL. Inflammasome Is Activated in the Liver of Cholestatic Patients and Aggravates Hepatic Injury in Bile Duct–Ligated Mouse. Cell Mol Gastroenterol Hepatol [Internet]. Elsevier; 2020 [cited 2022 Mar 16];9:679. Available from: /pmc/articles/PMC7160576/

53. Taylor SA, Chen S-Y, Gadhvi G, Feng L, Gromer KD, Abdala-Valencia H, et al. Transcriptional profiling of pediatric cholestatic livers identifies three distinct macrophage populations. PLoS One [Internet]. Public Library of Science; 2021 [cited 2021 Aug 2];16:e0244743. Available from: https://journals.plos.org/plosone/article?id=10.1371/journal.pone.0244743

54. Radtke F, Fasnacht N, MacDonald HR. Notch Signaling in the Immune System. Immunity. Cell Press; 2010. p. 14–27.

55. Radtke F, Ferrero I, Wilson A, Lees R, Aguet M, MacDonald HR. Notch1 deficiency dissociates the intrathymic development of dendritic cells and T cells. J Exp Med [Internet]. The Rockefeller University Press; 2000 [cited 2020 Aug 23];191:1085–93. Available from: http://www.jem.org/cgi/current/full/191/7/1085

56. Martín-Gayo E, González-García S, García-León MJ, Murcia-Ceballos A, Alcain J, García-Peydró M, et al. Spatially restricted JAG1-Notch signaling in human thymus provides suitable DC developmental niches. J Exp Med [Internet]. Rockefeller University Press; 2017 [cited 2020 Nov 29];214:3361–79. Available from: https://doi.org/10.1084/jem.20161564

57. Weijzen S, Velders MP, Elmishad AG, Bacon PE, Panella JR, Nickoloff BJ, et al. The Notch Ligand Jagged-1 Is Able to Induce Maturation of Monocyte-Derived Human Dendritic Cells. J Immunol [Internet]. The American Association of Immunologists; 2002 [cited 2020 Jul 28];169:4273–8. Available from: http://www.jimmunol.org/content/169/8/4273http://www.jimmunol.org/content/169/8/4273.full#ref-list-1

58. Bachanova V, McCullar V, Lenvik T, Wangen R, Peterson KA, Ankarlo DEM, et al. Activated Notch Supports Development of Cytokine Producing NK Cells Which Are Hyporesponsive and Fail to Acquire NK Cell Effector Functions. Biol Blood Marrow Transplant [Internet]. Elsevier; 2009 [cited 2019 Dec 6];15:183–94. Available from: https://www.sciencedirect.com/science/article/pii/S108387910800579X?via%3Dihub

59. Poulos MG, Guo P, Kofler NM, Pinho S, Gutkin MC, Tikhonova A, et al. Endothelial Jagged-1 Is necessary for homeostatic and regenerative hematopoiesis. Cell Rep [Internet]. 2013 [cited 2020 Jul 28];4:1022–34. Available from: https://pubmed.ncbi.nlm.nih.gov/24012753/

60. Le Friec G, Sheppard D, Whiteman P, Karsten CM, Shamoun SA-T, Laing A, et al. The CD46-Jagged1 interaction is critical for human TH1 immunity. Nat Immunol [Internet]. Nature Publishing Group; 2012 [cited 2016 Mar 31];13:1213–21. Available from: http://www.nature.com/articles/ni.2454

61. Andersson ER, Chivukula I V., Hankeova S, Sjöqvist M, Tsoi YL, Ramsköld D, et al. Mouse Model of Alagille Syndrome and Mechanisms of Jagged1 Missense Mutations. Gastroenterology. W.B. Saunders; 2018;154:1080–95.

62. Hankeova S, Salplachta J, Zikmund T, Kavkova M, Van Hul N, Brinek A, et al. Duct reveals architectural mechanisms contributing to bile duct recovery in a mouse model for alagille syndrome. Elife. eLife Sciences Publications Ltd; 2021;10:1–29.

63. Andervont HB. Studies on the occurrence of spontaneous hepatomas in mice of strains c3h and cba. J Natl Cancer Inst [Internet]. 1950 [cited 2014 Feb 4];11:581–92. Available from: http://www.ncbi.nlm.nih.gov/pubmed/14824917

64. Tamano S, Hagiwara A, Shibata MA, Kurata Y, Fukushima S, Ito N. Spontaneous tumors in aging (C57BL/6N x C3H/HeN)F1 (B6C3F1) mice. Toxicol Pathol. 1988;16:321–6.

65. Calvisi DF, Factor VM, Ladu S, Conner EA, Thorgeirsson SS. Disruption of β-catenin pathway or genomic instability define two distinct categories of liver cancer in transgenic mice. Gastroenterology [Internet]. Elsevier; 2004 [cited 2022 Jun 6];126:1374–86. Available from: http://www.gastrojournal.org/article/S0016508504001945/fulltext

66. Ramakrishna G, Rastogi A, Trehanpati N, Sen B, Khosla R, Sarin SK. From Cirrhosis to Hepatocellular Carcinoma: New Molecular Insights on Inflammation and Cellular Senescence. Liver Cancer [Internet]. Karger Publishers; 2013 [cited 2022 Jun 6];2:367–83. Available from: https://www.karger.com/Article/FullText/343852

67. Garrido A, Djouder N. Cirrhosis: A Questioned Risk Factor for Hepatocellular Carcinoma. Trends in Cancer. Cell Press; 2021;7:29–36.

68. Schindler EA, Gilbert MA, Piccoli DA, Spinner NB, Krantz ID, Loomes KM. Alagille syndrome and risk for hepatocellular carcinoma: Need for increased surveillance in adults with mild liver phenotypes. Am J Med Genet Part A [Internet]. John Wiley and Sons Inc; 2021 [cited 2021 Feb 23];185:719–31. Available from: https://onlinelibrary.wiley.com/doi/10.1002/ajmg.a.62028

69. Emerick KM, Rand EB, Goldmuntz E, Krantz ID, Spinner NB, Piccoli DA. Features of Alagille syndrome in 92 patients: frequency and relation to prognosis. Hepatology [Internet]. W.B. Saunders; 1999 [cited 2016 Jul 7];29:822–9. Available from: http://doi.wiley.com/10.1002/hep.510290331

70. Gijbels E, Pieters A, De Muynck K, Vinken M, Devisscher L. Rodent models of cholestatic liver disease: A practical guide for translational research. Liver Int [Internet]. Wiley-Blackwell; 2021 [cited 2021 Aug 24];41:656–82. Available from: /pmc/articles/PMC8048655/

71. Butler A, Hoffman P, Smibert P, Papalexi E, Satija R. Integrating single-cell transcriptomic data across different conditions, technologies, and species. Nat Biotechnol. Nature Publishing Group; 2018;36:411–20.

72. Popescu DM, Botting RA, Stephenson E, Green K, Webb S, Jardine L, et al. Decoding human fetal liver haematopoiesis. Nature [Internet]. Nature Publishing Group; 2019 [cited 2019 Nov 17];574:365–71. Available from: http://www.nature.com/articles/s41586-019-1652-y

73. Wang X, Yang L, Wang YYYC, Xu ZR, Feng Y, Zhang J, et al. Comparative analysis of cell lineage differentiation during hepatogenesis in humans and mice at the single-cell transcriptome level. Cell Res [Internet]. Springer Nature; 2020 [cited 2020 Aug 3];1–18. Available from: https://doi.org/10.1038/s41422-020-0378-6

74. Guilliams M, Bonnardel J, Haest B, Vanderborght B, Wagner C, Remmerie A, et al. Spatial proteogenomics reveals distinct and evolutionarily conserved hepatic macrophage niches. Cell. Cell Press; 2022;185:379-396.e38.

75. Pellicci DG, Hammond KJL, Uldrich AP, Baxter AG, Smyth MJ, Godfrey DI. A natural killer T (NKT) cell developmental pathway involving a thymus-dependent NK1.1-CD4+ CD1d-dependent precursor stage. J Exp Med [Internet]. The Rockefeller University Press; 2002 [cited 2022 Jan 19];195:835–44. Available from: /pmc/articles/PMC2193721/

76. Hu Y, Fang K, Wang Y, Lu N, Sun H, Zhang C. Single-cell analysis reveals the origins and intrahepatic development of liver-resident IFN-γ-producing γδ T cells. Cell Mol Immunol [Internet]. Nature Publishing Group; 2021 [cited 2022 Jan 19];18:954–68. Available from: https://www.nature.com/articles/s41423-021-00656-1

77. Glasner A, Isaacson B, Viukov S, Neuman T, Friedman N, Mandelboim M, et al. Increased NK cell immunity in a transgenic mouse model of NKp46 overexpression. Sci Reports 2017 71 [Internet]. Nature Publishing Group; 2017 [cited 2022 Sep 29];7:1–9. Available from: https://www.nature.com/articles/s41598-017-12998-w

78. Tang Y, Peitzsch C, Charoudeh HN, Cheng M, Chaves P, Jacobsen

SEW, et al. Emergence of NK-cell progenitors and functionally competent NK-cell lineage subsets in the early mouse embryo. Blood [Internet]. American Society of Hematology; 2012 [cited 2022 Sep 29];120:63–75. Available from: https://ashpublications.org/blood/article/120/1/63/30143/Emergence-of-NK-cell-progenitors-and-functionally

79. Filipovic I, Sönnerborg I, Strunz B, Friberg D, Cornillet M, Hertwig L, et al. 29-Color Flow Cytometry: Unraveling Human Liver NK Cell Repertoire Diversity. Front Immunol. Frontiers Media S.A.; 2019;10:2692.

80. Patel AM, Liu YS, Davies SP, Brown RM, Kelly DA, Scheel-Toellner D, et al. The Role of B Cells in Adult and Paediatric Liver Injury. Front. Immunol. Frontiers Media S.A.; 2021. p. 3545.

81. Allen K, Jaeschke H, Copple BL. Bile Acids Induce Inflammatory Genes in Hepatocytes. Am J Pathol [Internet]. Elsevier; 2011 [cited 2022 Mar 16];178:175–86. Available from: https://linkinghub.elsevier.com/retrieve/pii/S0002944010000726

82. Gujral JS, Farhood A, Bajt ML, Jaeschke H. Neutrophils aggravate acute liver injury during obstructive cholestasis in bile duct-ligated mice. Hepatology [Internet]. Hepatology; 2003 [cited 2022 Mar 16];38:355–63. Available from: https://pubmed.ncbi.nlm.nih.gov/12883479/

83. Gao B, Radaeva S. Natural killer and natural killer T cells in liver fibrosis. Biochim Biophys Acta [Internet]. NIH Public Access; 2013 [cited 2022 Jan 19];1832:1061. Available from: /pmc/articles/PMC3552008/

84. Zhang M, Zhang S. T Cells in Fibrosis and Fibrotic Diseases. Front. Immunol. Frontiers; 2020. p. 1142.

85. Veillette A, Horak ID, Horak EM, Bookman MA, Bolen' JB. Alterations of the lymphocyte-specific protein tyrosine kinase (p56lck) during T-cell activation. Mol Cell Biol [Internet]. American Society for Microbiology (ASM); 1988 [cited 2022 Jun 6];8:4353. Available from: /pmc/articles/PMC365508/?report=abstract

86. Su T, Yang Y, Lai S, Jeong J, Jung Y, McConnell M, et al. Single-Cell Transcriptomics Reveals Zone-Specific Alterations of Liver Sinusoidal Endothelial Cells in Cirrhosis. CMGH [Internet]. Elsevier BV; 2021 [cited 2021 Mar 13];11:1139–61. Available from: https://doi.org/10.1016/j.jcmgh.2020.12.007

87. Ma R, Martínez-Ramírez AS, Borders TL, Gao F, Sosa-Pineda B. Metabolic and non-metabolic liver zonation is established non-synchronously and requires sinusoidal Wnts. Elife. eLife Sciences Publications Ltd; 2020;9.

88. Friedman SL, Roll FJ, Boyles J, Bissell DM. Hepatic lipocytes: the principal collagen-producing cells of normal rat liver. Proc Natl Acad Sci U S A [Internet]. National Academy of Sciences; 1985 [cited 2022 Aug 16];82:8681. Available from: /pmc/articles/PMC391500/?report=abstract

89. Tsuchida T, Friedman SL. Mechanisms of hepatic stellate cell activation. Nat Rev Gastroenterol Hepatol 2017 147 [Internet]. Nature Publishing Group; 2017 [cited 2022 Aug 16];14:397–411. Available from: https://www.nature.com/articles/nrgastro.2017.38

90. Kitto LJ, Henderson NC. Hepatic Stellate Cell Regulation of Liver Regeneration and Repair. Hepatol Commun [Internet]. Hepatol Commun; 2021 [cited 2021 Jul 20];5:358–70. Available from: https://pubmed.ncbi.nlm.nih.gov/33681672/

91. Ben-Moshe S, Shapira Y, Moor AE, Manco R, Veg T, Bahar Halpern K, et al. Spatial sorting enables comprehensive characterization of liver zonation. Nat Metab [Internet]. Nature Research; 2019 [cited 2021 Feb 28];1:899–911. Available from: https://doi.org/10.1038/s42255-019-0109-9

92. Halpern KB, Shenhav R, Matcovitch-Natan O, Tóth B, Lemze D, Golan M, et al. Single-cell spatial reconstruction reveals global division of labour in the mammalian liver. Nat 2017 5427641 [Internet]. Nature Publishing Group; 2017 [cited 2022 Mar 17];542:352–6. Available from: https://www.nature.com/articles/nature21065

93. Cao J, Spielmann M, Qiu X, Huang X, Ibrahim DM, Hill AJ, et al. The single-cell transcriptional landscape of mammalian organogenesis. Nature [Internet]. Nature Publishing Group; 2019 [cited 2019 Apr 2];566:496–502. Available from: http://www.nature.com/articles/s41586-019-0969-x

94. Weinstein M, Monga SPS, Liu Y, Brodie SG, Tang Y, Li C, et al. Smad Proteins and Hepatocyte Growth Factor Control Parallel Regulatory Pathways That Converge on β1-Integrin To Promote Normal Liver Development. Mol Cell Biol [Internet]. American Society for Microbiology; 2001 [cited 2022 Mar 18];21:5122–31. Available from: https://journals.asm.org/doi/abs/10.1128/MCB.21.15.5122-5131.2001

95. Dennler S, Prunier C, Ferrand N, Gauthier JM, Atfi A. c-Jun Inhibits Transforming Growth Factor β-mediated Transcription by Repressing Smad3 Transcriptional Activity *. J Biol Chem [Internet]. Elsevier; 2000 [cited 2022 Mar 18];275:28858–65. Available from: http://www.jbc.org/article/S0021925819612706/fulltext

96. Clotman F, Jacquemin P, Plumb-Rudewiez N, Pierreux CE, Van Der Smissen P, Dietz HC, et al. Control of liver cell fate decision by a gradient of TGFβ signaling modulated by Onecut transcription factors. Genes Dev [Internet]. Cold Spring Harbor Laboratory Press; 2005 [cited 2022 Mar 18];19:1849–54. Available from: http://genesdev.cshlp.org/content/19/16/1849.full

97. Van Dam H, Castellazzi M. Distinct roles of Jun : Fos and Jun : ATF dimers in oncogenesis. Oncogene 2001 2019 [Internet]. Nature Publishing Group; 2001 [cited 2022 Mar 18];20:2453–64. Available from: https://www.nature.com/articles/1204239

98. Yu G, Wang LG, Han Y, He QY. ClusterProfiler: An R package for comparing biological themes among gene clusters. Omi A J Integr Biol [Internet]. Mary Ann Liebert, Inc. 140 Huguenot Street, 3rd Floor New Rochelle, NY 10801 USA ; 2012 [cited 2022 Mar 18];16:284–7. Available from: https://www.liebertpub.com/doi/abs/10.1089/omi.2011.0118

99. Zhang Y, Feng XH, Derynck R. Smad3 and Smad4 cooperate with c-Jun/c-Fos to mediate TGF-β-induced transcription. Nat 1998 3946696 [Internet]. Nature Publishing Group; 1998 [cited 2022 Oct 20];394:909–13. Available from: https://www.nature.com/articles/29814

100. Kong B, Michalski CW, Hong X, Valkovskaya N, Rieder S, Abiatari I, et al. AZGP1 is a tumor suppressor in pancreatic cancer inducing mesenchymal-to-epithelial transdifferentiation by inhibiting TGF-β-mediated ERK signaling. Oncogene 2010 2937 [Internet]. Nature Publishing Group; 2010 [cited 2022 Feb 1];29:5146–58. Available from: https://www.nature.com/articles/onc2010258

101. Tian H, Ge C, Zhao F, Zhu M, Zhang L, Huo Q, et al. Downregulation of AZGP1 by Ikaros and histone deacetylase promotes tumor progression through the PTEN/Akt and CD44s pathways in hepatocellular carcinoma. Carcinogenesis [Internet]. Carcinogenesis; 2017 [cited 2022 Feb 20];38:207–17. Available from: https://pubmed.ncbi.nlm.nih.gov/27993894/

102. Zhang Y, Csanaky IL, Cheng X, Lehman-McKeeman LD, Klaassen CD. Organic Anion Transporting Polypeptide 1a1 Null Mice Are Sensitive to Cholestatic Liver Injury. Toxicol Sci [Internet]. Oxford Academic; 2012 [cited 2022 Mar 18];127:451–62. Available from: https://academic.oup.com/toxsci/article/127/2/451/1711117

103. Li S, Wang C, Zhang X, Su W. Cytochrome P450 Omega-Hydroxylase 4a14 Attenuates Cholestatic Liver Fibrosis. Front Physiol. Frontiers Media S.A.; 2021;12:692.

104. Sullivan BP, Weinreb PH, Violette SM, Luyendyk JP. The coagulation system contributes to alphaVbeta6 integrin expression and liver fibrosis induced by cholestasis. Am J Pathol [Internet]. Am J Pathol; 2010 [cited 2022 Mar 18];177:2837–49. Available from: https://pubmed.ncbi.nlm.nih.gov/21037076/

105. Kopec AK, Luyendyk JP. Role of Fibrin(ogen) in Progression of Liver Disease: Guilt by Association? Semin Thromb Hemost [Internet]. NIH Public Access; 2016 [cited 2022 Mar 18];42:397. Available from: /pmc/articles/PMC5338033/

106. Oldenborg PA, Zheleznyak A, Fang YF, Lagenaur CF, Gresham HD, Lindberg FP. Role of CD47 as a marker of self on red blood cells. Science [Internet]. Science; 2000 [cited 2022 Mar 18];288:2051–4. Available from: https://pubmed.ncbi.nlm.nih.gov/10856220/

107. Jaiswal S, Jamieson CHM, Pang WW, Park CY, Chao MP, Majeti R, et al. CD47 is upregulated on circulating hematopoietic stem cells and leukemia cells to avoid phagocytosis. Cell [Internet]. Cell; 2009 [cited 2022 Mar 18];138:271–85. Available from: https://pubmed.ncbi.nlm.nih.gov/19632178/

108. Vaeteewoottacharn K, Kariya R, Pothipan P, Fujikawa S, Pairojkul

C, Waraasawapati S, et al. Attenuation of CD47-SIRPα Signal in Cholangiocarcinoma Potentiates Tumor-Associated Macrophage-Mediated Phagocytosis and Suppresses Intrahepatic Metastasis. Transl Oncol [Internet]. Neoplasia Press; 2019 [cited 2022 Mar 18];12:217. Available from: /pmc/articles/PMC6231245/

109. Wang X, Park J, Susztak K, Zhang NR, Li M. Bulk tissue cell type deconvolution with multi-subject single-cell expression reference. Nat Commun 2019 101 [Internet]. Nature Publishing Group; 2019 [cited 2022 Jun 5];10:1–9. Available from: https://www.nature.com/articles/s41467-018-08023-x

110. Cortegano I, Melgar-Rojas P, Luna-Zurita L, Siguero-Álvarez M, Marcos MA, Gaspar ML, et al. Notch1 regulates progenitor cell proliferation and differentiation during mouse yolk sac hematopoiesis. Cell Death Differ [Internet]. Nature Publishing Group; 2014 [cited 2021 Mar 9];21:1081–94. Available from: https://pubmed.ncbi.nlm.nih.gov/24583642/

111. Li J, Gordon J, Chen ELY, Xiao S, Wu L, Zúniga-Pflücker JC, et al. NOTCH1 signaling establishes the medullary thymic epithelial cell progenitor pool during mouse fetal development. Dev. Company of Biologists Ltd; 2020;147.

112. Liu D, Kousa AI, O'Neill KE, Rouse P, Popis M, Farley AM, et al. Canonical Notch signaling controls the early thymic epithelial progenitor cell state and emergence of the medullary epithelial lineage in fetal thymus development. Dev [Internet]. Company of Biologists Ltd; 2020 [cited 2021 May 11];147. Available from: /pmc/articles/PMC7328009/

113. Van de Walle I, Waegemans E, De Medts J, De Smet G, De Smedt M, Snauwaert S, et al. Specific notch receptor-ligand interactions control human TCR-αβ/γδ development by inducing differential notch signal strength. J Exp Med [Internet]. 2013 [cited 2021 Nov 21];210:683–97. Available from: www.jem.org/cgi/doi/10.1084/jem.20121798

114. Van De Walle I, De Smet G, Gärtner M, De Smedt M, Waegemans E, Vandekerckhove B, et al. Jagged2 acts as a Delta-like Notch ligand during early hematopoietic cell fate decisions. Blood [Internet]. Blood; 2011 [cited 2021 Dec 16];117:4449–59. Available from: https://pubmed.ncbi.nlm.nih.gov/21372153/

115. Garcıá-Leoń MJ, Fuentes P, de la Pompa JL, Toribio ML. Dynamic regulation of NOTCH1 activation and notch ligand expression in human thymus development. Dev [Internet]. Company of Biologists Ltd; 2018 [cited 2020 Nov 29];145. Available from: https://dev.biologists.org/content/145/16/dev165597

116. Felli MP, Maroder M, Mitsiadis TA, Campese AF, Bellavia D, Vacca A, et al. Expression pattern of notch1, 2 and 3 and Jagged1 and 2 in lymphoid and stromal thymus components: distinct ligand-receptor interactions in intrathymic T cell development. Int Immunol [Internet]. Int Immunol; 1999 [cited 2022 Jun 6];11:1017–25. Available from: https://pubmed.ncbi.nlm.nih.gov/10383933/

117. Anderson G, Pongracz J, Parnell S, Jenkinson EJ. Notch ligand-bearing thymic epithelial cells initiate and sustain Notch signaling in thymocytes independently of T cell receptor signaling. Eur J Immunol. 2001;31:3349–54.

118. Lehar SM, Dooley J, Farr AG, Bevan MJ. Notch ligands Delta1 and Jagged1 transmit distinct signals to T-cell precursors. Blood [Internet]. American Society of Hematology; 2005 [cited 2022 Jun 6];105:1440–7. Available from: https://ashpublications.org/blood/article/105/4/1440/20383/Notch-ligands-Delta1-and-Jagged1-transmit-distinct

119. Park JE, Botting RA, Conde CD, Popescu DM, Lavaert M, Kunz DJ, et al. A cell atlas of human thymic development defines T cell repertoire formation. Science (80-) [Internet]. American Association for the Advancement of Science; 2020 [cited 2021 Dec 16];367. Available from: https://www.science.org/doi/abs/10.1126/science.aay3224

120. Alagille D, Estrada A, Hadchouel M, Gautler M, Odièvre M, Dommergues JP, et al. Syndromic paucity of interlobular bile ducts (Alagille syndrome or arteriohepatic dysplasia): Review of 80 cases. J Pediatr [Internet]. 1987 [cited 2015 Aug 13];110:195–200. Available from: http://www.ncbi.nlm.nih.gov/pubmed/3806290

121. Morali GA, Blendis LM. Splenomegaly in Portal Hypertension: Causes and Effects. Portal Hypertens [Internet]. Springer, Tokyo; 1991 [cited 2022 Oct 8];85–99. Available from: https://link.springer.com/chapter/10.1007/978-4-431-68361-2_7

122. Giovannetti A, Pierdominici M, Mazzetta F, Marziali M, Renzi C, Mileo AM, et al. Unravelling the Complexity of T Cell Abnormalities in Common Variable Immunodeficiency. J Immunol [Internet]. American Association of Immunologists; 2007 [cited 2022 Oct 9];178:3932–43. Available from: https://www.jimmunol.org/content/178/6/3932

123. Burghardt S, Erhardt A, Claass B, Huber S, Adler G, Jacobs T, et al. Hepatocytes Contribute to Immune Regulation in the Liver by Activation of the Notch Signaling Pathway in T Cells. J Immunol [Internet]. The American Association of Immunologists; 2013 [cited 2020 Jul 28];191:5574–82. Available from: www.jimmunol.org/cgi/doi/10.4049/jimmunol.1300826

124. Mombaerts P, Iacomini J, Johnson RS, Herrup K, Tonegawa S, Papaioannou VE. RAG-1-deficient mice have no mature B and T lymphocytes. Cell. Cell Press; 1992;68:869–77.

125. Ostanin D V., Bao J, Koboziev I, Gray L, Robinson-Jackson SA, Kosloski-Davidson M, et al. T cell transfer model of chronic colitis: concepts, considerations, and tricks of the trade. https://doi.org/101152/ajpgi904622008 [Internet]. American Physiological Society; 2009 [cited 2021 Jul 30];296:135–46. Available from: https://journals.physiology.org/doi/abs/10.1152/ajpgi.90462.2008

126. Mottet C, Uhlig HH, Powrie F. Cutting edge: cure of colitis by CD4+CD25+ regulatory T cells. J Immunol [Internet]. J Immunol; 2003 [cited 2022 Oct 19];170:3939–43. Available from: https://pubmed.ncbi.nlm.nih.gov/12682220/

127. Erben U, Loddenkemper C, Doerfel K, Spieckermann S, Haller D, Heimesaat MM, et al. A guide to histomorphological evaluation of intestinal inflammation in mouse models. Int J Clin Exp Pathol [Internet]. e-Century Publishing Corporation; 2014 [cited 2021 Sep 6];7:4557–76. Available from: /pmc/articles/PMC4152019/

128. Fickert P, Stöger U, Fuchsbichler A, Moustafa T, Marschall HU, Weiglein AH, et al. A New Xenobiotic-Induced Mouse Model of Sclerosing Cholangitis and Biliary Fibrosis. Am J Pathol. Elsevier; 2007;171:525–36.

129. Dobie R, Wilson-Kanamori JR, Henderson BEP, Smith JR, Matchett KP, Portman JR, et al. Single-Cell Transcriptomics Uncovers Zonation of Function in the Mesenchyme during Liver Fibrosis. Cell Rep. Elsevier B.V.; 2019;29:1832-1847.e8.

130. Chassaing B, Aitken JD, Malleshappa M, Vijay-Kumar M. Dextran Sulfate Sodium (DSS)-Induced Colitis in Mice. Curr Protoc Immunol [Internet]. NIH Public Access; 2014 [cited 2022 Oct 20];104:Unit. Available from: /pmc/articles/PMC3980572/

131. Perše M, Cerar A. Dextran sodium sulphate colitis mouse model: Traps and tricks. J Biomed Biotechnol. 2012;2012.

132. Henderson NC, Rieder F, Wynn TA. Fibrosis: from mechanisms to medicines [Internet]. Nature. Nature Publishing Group; 2020 [cited 2021 Jul 30]. p. 555–66. Available from: https://www.nature.com/articles/s41586-020-2938-9

133. Fabris L, Spirli C, Cadamuro M, Fiorotto R, Strazzabosco M. Emerging concepts in biliary repair and fibrosis [Internet]. Am. J. Physiol. - Gastrointest. Liver Physiol. American Physiological Society; 2017 [cited 2021 Dec 23]. p. G102–16. Available from: https://journals.physiology.org/doi/abs/10.1152/ajpgi.00452.2016

134. Robinson MW, Harmon C, O'Farrelly C. Liver immunology and its role in inflammation and homeostasis. Cell Mol Immunol 2016 133 [Internet]. Nature Publishing Group; 2016 [cited 2022 Oct 20];13:267–76. Available from: https://www.nature.com/articles/cmi20163

135. Pinzani M, Luong TV. Pathogenesis of biliary fibrosis. Biochim Biophys Acta - Mol Basis Dis. Elsevier; 2018;1864:1279–83.

136. Tam PKH, Yiu RS, Lendahl U, Andersson ER. Cholangiopathies – Towards a molecular understanding [Internet]. EBioMedicine. Elsevier B.V.; 2018 [cited 2021 Mar 15]. p. 381–93. Available from: https://doi.org/10.1016/j.ebiom.2018.08.024

137. Khandekar G, Llewellyn J, Kriegermeier A, Waisbourd-Zinman O, Johnson N, Du Y, et al. Coordinated development of the mouse extrahepatic bile duct: Implications for neonatal susceptibility to biliary injury. J Hepatol. Elsevier; 2020;72:135–45.

138. Ader T, Norel R, Levoci L, Rogler LE. Transcriptional profiling implicates TGFβ/BMP and Notch signaling pathways in ductular differentiation of fetal murine hepatoblasts. Mech Dev. Elsevier; 2006;123:177–94.

139. Goessling W, North TE, Lord AM, Ceol C, Lee S, Weidinger G, et al. APC mutant zebrafish uncover a changing temporal requirement for wnt signaling in liver development. Dev Biol [Internet]. 2008 [cited 2016 Nov 2];320:161–74. Available from: http://www.ncbi.nlm.nih.gov/pubmed/18585699

140. Suksaweang S, Lin CM, Jiang TX, Hughes MW, Widelitz RB, Chuong CM. Morphogenesis of chicken liver: identification of localized growth zones and the role of β-catenin/Wnt in size regulation. Dev Biol. Academic Press; 2004;266:109–22.

141. Berg T, Rountree CB, Lee L, Estrada J, Sala FG, Choe A, et al. Fibroblast growth factor 10 is critical for liver growth during embryogenesis and controls hepatoblast survival via β-catenin activation. Hepatology [Internet]. John Wiley & Sons, Ltd; 2007 [cited 2022 Sep 26];46:1187–97. Available from: https://onlinelibrary.wiley.com/doi/full/10.1002/hep.21814

142. Schmidt C, Bladt F, Goedecke S, Brinkmann V, Zschiesche W, Sharpe M, et al. Scatter factor/hepatocyte growth factor is essential for liver development. Nat 1995 3736516 [Internet]. Nature Publishing Group; 1995 [cited 2022 Sep 26];373:699–702. Available from: https://www.nature.com/articles/373699a0

143. Lee D-H, Park JO, Kim TT-S, Kim S-KS-Y, Kim TT-S, Kim M, et al. LATS-YAP/TAZ controls lineage specification by regulating TGFβ signaling and Hnf4α expression during liver development. Nat Commun [Internet]. Nature Publishing Group; 2016;7:11961. Available from: http://www.nature.com/doifinder/10.1038/ncomms11961

144. Camargo FD, Gokhale S, Johnnidis JB, Fu D, Bell GW, Jaenisch R, et al. YAP1 Increases Organ Size and Expands Undifferentiated Progenitor Cells. Curr Biol. Cell Press; 2007;17:2054–60.

145. Yang L, Wang WH, Qiu WL, Guo Z, Bi E, Xu CR. A single-cell transcriptomic analysis reveals precise pathways and regulatory mechanisms underlying hepatoblast differentiation. Hepatology [Internet]. 2017 [cited 2017 Sep 20];66:1387–401. Available from: http://doi.wiley.com/10.1002/hep.29353

146. Ryan MJ, Bales C, Nelson A, Gonzalez DM, Underkoffler L, Segalov M, et al. Bile duct proliferation in Jag1/fringe heterozygous mice identifies candidate modifiers of the Alagille syndrome hepatic phenotype. Hepatology [Internet]. Hepatology; 2008 [cited 2021 Mar 27];48:1989–97. Available from: https://pubmed.ncbi.nlm.nih.gov/19026002/

147. Loomes KM, Russo P, Ryan M, Nelson A, Underkoffler L, Glover C, et al. Bile duct proliferation in liver-specific Jag1 conditional knockout mice: Effects of gene dosage. Hepatology [Internet]. Hepatology; 2007 [cited 2021 Jun 30];45:323–30. Available from: https://pubmed.ncbi.nlm.nih.gov/17366661/

148. McCright B, Lozier J, Gridley T, Grochowski CM, Loomes KM, Spinner NB, et al. A mouse model of Alagille syndrome: Notch2 as a genetic modifier of Jag1 haploinsufficiency. Gene [Internet]. The Company of Biologists Ltd; 2002 [cited 2013 Sep 4];10:1075–82. Available from: http://www.ncbi.nlm.nih.gov/pubmed/9207787%5Cnhttp://www.nature.com/ng/journal/v16/n3/pdf/ng0797-235.pdf%5Cnhttp://www.ncbi.nlm.nih.gov/pubmed/11157803%5Cn http://www.nature.com/doifinder/10.1038/ejhg.2013.140%5Cnhttp://dx.doi.org/10.1016/j.gene.2015.10.065

149. Takayama K, Kawabata K, Nagamoto Y, Inamura M, Ohashi K, Okuno H, et al. CCAAT/enhancer binding protein-mediated regulation of TGFβ receptor 2 expression determines the hepatoblast fate decision. Development [Internet]. The Company of Biologists; 2014 [cited 2022 Sep 27];141:91–100. Available from: https://journals.biologists.com/dev/article/141/1/91/46142/CCAAT-enhancer-binding-protein-mediated-regulation

150. Sahoo S, Mishra A, Diehl AM, Jolly MK. Dynamics of hepatocyte-cholangiocyte cell-fate decisions during liver development and regeneration. iScience. Elsevier; 2022;25:104955.

151. Zhu HJ, Ding HH, Deng JY, Pan H, Wang LJ, Li NS, et al. Inhibition of preadipocyte differentiation and adipogenesis by zinc-α2-glycoprotein treatment in 3T3-L1 cells. J Diabetes Investig [Internet]. Wiley-Blackwell; 2013 [cited 2022 Sep 27];4:252. Available from: /pmc/articles/PMC4015661/

152. Xu MY, Chen R, Yu JX, Liu T, Qu Y, Lu LG. AZGP1 suppresses epithelial-to-mesenchymal transition and hepatic carcinogenesis by blocking TGFβ1-ERK2 pathways. Cancer Lett [Internet]. Cancer Lett; 2016 [cited 2022 Sep 27];374:241–9. Available from: https://pubmed.ncbi.nlm.nih.gov/26902423/

153. Liu Y, Wang T, Liu X, Wei X, Xu T, Yin M, et al. Neuronal zinc-α2-glycoprotein is decreased in temporal lobe epilepsy in patients and rats. Neuroscience [Internet]. Neuroscience; 2017 [cited 2022 Sep 27];357:56–66. Available from: https://pubmed.ncbi.nlm.nih.gov/28576733/

154. Kwon OJ, Valdez JM, Zhang L, Zhang B, Wei X, Su Q, et al. Increased Notch signalling inhibits anoikis and stimulates proliferation of prostate luminal epithelial cells. Nat Commun 2014 51 [Internet]. Nature Publishing Group; 2014 [cited 2022 Sep 27];5:1–15. Available from: https://www.nature.com/articles/ncomms5416

155. Kaylan KB, Berg IC, Biehl MJ, Brougham-Cook A, Jain I, Jamil SM, et al. Spatial patterning of liver progenitor cell differentiation mediated by cellular contractility and Notch signaling. Elife. eLife Sciences Publications Ltd; 2018;7.

156. Gashler A, Sukhatme VP. Early growth response protein 1 (Egr-1): prototype of a zinc-finger family of transcription factors. Prog Nucleic Acid Res Mol Biol [Internet]. Prog Nucleic Acid Res Mol Biol; 1995 [cited 2022 Sep 27];50:191–224. Available from: https://pubmed.ncbi.nlm.nih.gov/7754034/

157. Tao W, Wu J, Zhang Q, Lai SS, Jiang S, Jiang C, et al. EGR1 regulates hepatic clock gene amplitude by activating Per1 transcription. Sci Rep [Internet]. Nature Publishing Group; 2015 [cited 2022 Sep 27];5:1–13. Available from: https://www.nature.com/articles/srep15212

158. Wang W, Yu S, Zimmerman G, Wang Y, Myers J, Yu VWC, et al. Notch Receptor-Ligand Engagement Maintains Hematopoietic Stem Cell Quiescence and Niche Retention. Stem Cells [Internet]. NIH Public Access; 2015 [cited 2022 Mar 16];33:2280. Available from: /pmc/articles/PMC4478168/

159. Zhu C, Kim KJ, Wang X, Bartolome A, Salomao M, Dongiovanni P, et al. Hepatocyte Notch activation induces liver fibrosis in nonalcoholic steatohepatitis. Sci Transl Med. American Association for the Advancement of Science; 2018;10.

160. Schwabe RF, Tabas I, Pajvani UB. Mechanisms of Fibrosis Development in Nonalcoholic Steatohepatitis. Gastroenterology. W.B. Saunders; 2020;158:1913–28.

161. Cowan JE, Takahama Y, Bhandoola A, Ohigashi I. Postnatal Involution and Counter-Involution of the Thymus. Front Immunol. Frontiers Media S.A.; 2020;11:897.

162. García-León MJ, Mosquera M, Cela C, Alcain J, Zuklys S, Holländer G, et al. Abrogation of Notch Signaling in Embryonic TECs Impacts Postnatal mTEC Homeostasis and Thymic Involution. Front Immunol [Internet]. Frontiers; 2022 [cited 2022 Jun 2];13:2532. Available from: https://www.frontiersin.org/articles/10.3389/fimmu.2022.867302/full

163. Schmitt TM, Zúñiga-Pflücker JC. Induction of T cell development from hematopoietic progenitor cells by delta-like-1 in vitro. Immunity [Internet]. Immunity; 2002 [cited 2022 Sep 30];17:749–56. Available from: https://pubmed.ncbi.nlm.nih.gov/12479821/

164. Tanigaki K, Tsuji M, Yamamoto N, Han H, Tsukada J, Inoue H, et al. Regulation of αβ/γδ T Cell Lineage Commitment and Peripheral T Cell Responses by Notch/RBP-J Signaling. Immunity. Cell Press; 2004;20:611–22.

165. Koch U, Fiorini E, Benedito R, Besseyrias V, Schuster-Gossler K, Pierres M, et al. Delta-like 4 is the essential, nonredundant ligand for Notch1 during thymic T cell lineage commitment. J Exp Med [Internet]. The Rockefeller University Press; 2008 [cited 2022 Oct 8];205:2515–23. Available from: www.jem.org/cgi/doi/10.1084/jem.20080829

166. Izon DJ, Punt JA, Xu L, Karnell FG, Allman D, Myung PS, et al. Notch1 Regulates Maturation of CD4+ and CD8+ Thymocytes by Modulating TCR Signal Strength. Immunity. Cell Press; 2001;14:253–64.

167. Radtke F, Wilson A, Stark G, Bauer M, Van Meerwijk J, MacDonald HR, et al. Deficient T Cell Fate Specification in Mice with an Induced

Inactivation of Notch1. Immunity. Cell Press; 1999;10:547–58.

168. Hozumi K, Negishi N, Tsuchiya I, Abe N, Hirano K, Suzuki D, et al. Notch signaling is necessary for GATA3 function in the initiation of T cell development. Eur J Immunol [Internet]. John Wiley & Sons, Ltd; 2008 [cited 2020 Nov 29];38:977–85. Available from: http://doi.wiley.com/10.1002/eji.200737688

169. Jaleco AC, Neves H, Hooijberg E, Gameiro P, Clode N, Haury M, et al. Differential Effects of Notch Ligands Delta-1 and Jagged-1 in Human Lymphoid Differentiation. J Exp Med [Internet]. The Rockefeller University Press; 2001 [cited 2022 Jun 6];194:991–1002. Available from: http://www.jem.org/cgi/content/full/194/7/991

170. Ou-Yang HF, Zhang HW, Wu CG, Zhang P, Zhang J, Li JC, et al. Notch signaling regulates the FOXP3 promoter through RBP-J- and Hes1-dependent mechanisms. Mol Cell Biochem [Internet]. Mol Cell Biochem; 2009 [cited 2022 Oct 9];320:109–14. Available from: https://pubmed.ncbi.nlm.nih.gov/18777163/

171. Kritikou JS, Sánchez-Pascual I, Muñoz-Miranda JP, Vashist N, Wagner AK, Zhang X-M, et al. Jagged1 overexpression on T cells induces thymic regulatory T cells leading to thymic involution. bioRxiv [Internet]. Cold Spring Harbor Laboratory; 2022 [cited 2022 Oct 8];2022.08.25.504005. Available from: https://www.biorxiv.org/content/10.1101/2022.08.25.504005v1

172. Assarsson E, Chambers BJ, Högstrand K, Berntman E, Lundmark C, Fedorova L, et al. Severe Defect in Thymic Development in an Insertional Mutant Mouse Model. J Immunol [Internet]. American Association of Immunologists; 2007 [cited 2022 Oct 8];178:5018–27. Available from: https://www.jimmunol.org/content/178/8/5018

173. Lin CL, Huang HM, Hsieh CL, Fan CK, Lee YL. Jagged1-expressing adenovirus-infected dendritic cells induce expansion of Foxp3+ regulatory T cells and alleviate T helper type 2-mediated allergic asthma in mice. Immunology [Internet]. Immunology; 2019 [cited 2022 Oct 7];156:199–212. Available from: https://pubmed.ncbi.nlm.nih.gov/30418664/

174. Burghardt S, Claass B, Erhardt A, Karimi K, Tiegs G. Hepatocytes induce Foxp3+ regulatory T cells by Notch signaling. J Leukoc Biol [Internet]. John Wiley & Sons, Ltd; 2014 [cited 2022 Oct 9];96:571–7. Available from: https://onlinelibrary.wiley.com/doi/full/10.1189/jlb.2AB0613-342RR

175. Cahill EF, Tobin LM, Carty F, Mahon BP, English K. Jagged-1 is required for the expansion of CD4+ CD25+ FoxP3+ regulatory T cells and tolerogenic dendritic cells by murine mesenchymal stromal cells. Stem Cell Res Ther [Internet]. BioMed Central Ltd.; 2015 [cited 2020 Jul 28];6:19. Available from: http://stemcellres.com/content/6/1/19

176. Kumar P, Alharshawi K, Bhattacharya P, Marinelarena A, Haddad C, Sun Z, et al. Soluble OX40L and JAG1 Induce Selective Proliferation of Functional Regulatory T-Cells Independent of canonical TCR signaling. Sci Rep [Internet]. Sci Rep; 2017 [cited 2022 Oct 7];7. Available from: https://pubmed.ncbi.nlm.nih.gov/28045060/

177. Kumar P, Lele SS, Ragothaman VK, Raghunathan D, Epstein AL, Chiba S, et al. OX40L-JAG1-Induced Expansion of Lineage-Stable Regulatory T Cells Involves Noncanonical NF-κB Signaling. J Immunol [Internet]. J Immunol; 2019 [cited 2022 Oct 7];203:3225–36. Available from: https://pubmed.ncbi.nlm.nih.gov/31704879/

178. Han Y, Bian ZH, Yang SY, Wang CB, Li L, Yang YQ, et al. Single-Cell Characterization of Hepatic CD8+ T Cells in a Murine Model of Primary Biliary Cholangitis. Front Immunol [Internet]. Front Immunol; 2022 [cited 2022 Oct 9];13. Available from: https://pubmed.ncbi.nlm.nih.gov/35514982/

179. Guo C, Zhu J, Pu CL, Deng YH, Zhang MM. Combinatory effects of hepatic CD8+ and NK lymphocytes in bile duct injury from biliary atresia. Pediatr Res 2012 716 [Internet]. Nature Publishing Group; 2012 [cited 2022 Oct 9];71:638–44. Available from: https://www.nature.com/articles/pr201217

180. Taylor AE, Carey AN, Kudira R, Lages CS, Shi T, Lam S, et al. Interleukin 2 Promotes Hepatic Regulatory T Cell Responses and Protects From Biliary Fibrosis in Murine Sclerosing Cholangitis. Hepatology [Internet]. Hepatology; 2018 [cited 2022 Oct 9];68:1905–21. Available from: https://pubmed.ncbi.nlm.nih.gov/29698570/

181. Roh YS, Park S, Lim CW, Kim B. Depletion of Foxp3+ Regulatory T Cells Promotes Profibrogenic Milieu of Cholestasis-Induced Liver Injury. Dig Dis Sci 2014 607 [Internet]. Springer; 2014 [cited 2021 Nov 4];60:2009–18. Available from: https://link.springer.com/article/10.1007/s10620-014-3438-2

182. Claassen MAA, de Knegt RJ, Tilanus HW, Janssen HLA, Boonstra A. Abundant numbers of regulatory T cells localize to the liver of chronic hepatitis C infected patients and limit the extent of fibrosis. J Hepatol [Internet]. J Hepatol; 2010 [cited 2022 Oct 9];52:315–21. Available from: https://pubmed.ncbi.nlm.nih.gov/20129690/

183. Fickert P, Thueringer A, Moustafa T, Silbert D, Gumhold J, Tsybrovskyy O, et al. The role of osteopontin and tumor necrosis factor alpha receptor-1 in xenobiotic-induced cholangitis and biliary fibrosis in mice. Lab Investig 2010 906 [Internet]. Nature Publishing Group; 2010 [cited 2022 Oct 9];90:844–52. Available from: https://www.nature.com/articles/labinvest201061

184. Georgiev P, Jochum W, Heinrich S, Jang JH, Nocito A, Dahm F, et al. Characterization of time-related changes after experimental bile duct ligation. Br J Surg [Internet]. Oxford Academic; 2008 [cited 2022 Oct 9]. p. 646–56. Available from: https://academic.oup.com/bjs/article/95/5/646/6142604

185. Licata LA, Nguyen CT, Burga RA, Falanga V, Espat NJ, Ayala A, et al. Biliary obstruction results in PD-1-dependent liver T cell dysfunction and acute inflammation mediated by Th17 cells and neutrophils. J Leukoc Biol [Internet]. Wiley-Blackwell; 2013 [cited 2021 Mar 23];94:813–23. Available from: https://pubmed.ncbi.nlm.nih.gov/23883516/

186. Quiros-Tejeira RE, Ament ME, Heyman MB, Martin MG, Rosenthal P, Hall TR, et al. Variable morbidity in alagille syndrome: a review of 43 cases. J Pediatr Gastroenterol Nutr [Internet]. 1999;29:431–7. Available from: http://ovidsp.ovid.com/ovidweb.cgi?T=JS&CSC=Y&NEWS=N&PAGE=fulltext&D=med4&AN=10512403

187. Cardone J, Le Friec G, Vantourout P, Roberts A, Fuchs A, Jackson I, et al. Complement regulator CD46 temporally regulates cytokine production by conventional and unconventional T cells. Nat Immunol 2010 119 [Internet]. Nature Publishing Group; 2010 [cited 2022 Oct 9];11:862–71. Available from: https://www.nature.com/articles/ni.1917

188. Mukhopadhyay S, Saha S, Chakraborty S, Prasad P, Ghosh A, Aich P. Differential colitis susceptibility of Th1- and Th2-biased mice: A multi-omics approach. PLoS One [Internet]. Public Library of Science; 2022 [cited 2022 Oct 8];17. Available from: /pmc/articles/PMC8906622/

189. Dongre A, Surampudi L, Lawlor RG, Fauq AH, Miele L, Golde TE, et al. Non-canonical Notch signaling drives activation and differentiation of peripheral CD4+ T cells. Front Immunol. Frontiers Research Foundation; 2014;5:54.

190. Mitra A, Shanthalingam S, Sherman HL, Singh K, Canakci M, Torres JA, et al. CD28 Signaling Drives Notch Ligand Expression on CD4 T Cells. Front Immunol. Frontiers Media S.A.; 2020;11:735.

191. Mack CL, Falta MT, Sullivan AK, Karrer F, Sokol RJ, Freed BM, et al. Oligoclonal Expansions of CD4+ and CD8+ T-Cells in the Target Organ of Patients With Biliary Atresia. Gastroenterology [Internet]. W.B. Saunders; 2007 [cited 2020 Dec 13];133:278–87. Available from: https://pubmed.ncbi.nlm.nih.gov/17631149/

192. Taylor SA, Malladi P, Pan X, Wechsler JB, Hulse KE, Perlman H, et al. Oligoclonal immunoglobulin repertoire in biliary remnants of biliary atresia. Sci Rep [Internet]. Nature Publishing Group; 2019 [cited 2022 Oct 9];9. Available from: /pmc/articles/PMC6418100/

193. Bednarek J, Traxinger B, Brigham D, Roach J, Orlicky D, Wang D, et al. Cytokine-Producing B Cells Promote Immune-Mediated Bile Duct Injury in Murine Biliary Atresia. Hepatology [Internet]. John Wiley & Sons, Ltd; 2018 [cited 2022 Aug 22];68:1890–904. Available from: https://onlinelibrary.wiley.com/doi/full/10.1002/hep.30051

194. Lua I, Li Y, Zagory JA, Wang KS, French SW, Sévigny J, et al. Characterization of hepatic stellate cells, portal fibroblasts, and mesothelial cells in normal and fibrotic livers. J Hepatol [Internet]. J Hepatol; 2016 [cited 2022 Oct 21];64:1137–46. Available from: https://pubmed.ncbi.nlm.nih.gov/26806818/

195. Iwaisako K, Jiang C, Zhang M, Cong M, Moore-Morris TJ, Park TJ, et al. Origin of myofibroblasts in the fibrotic liver in mice. Proc Natl Acad Sci U S A [Internet]. National Academy of Sciences; 2014 [cited 2022 Oct 21];111. Available from: https://pubmed.ncbi.nlm.nih.gov/25074909/

196. Balounová J, Šplíchalová I, Dobešová M, Kolář M, Fišer K, Procházka J, et al. Toll-like receptor 2 expression on c-kit+ cells tracks the emergence of embryonic definitive hematopoietic progenitors. Nat Commun 2019 101 [Internet]. Nature Publishing Group; 2019 [cited 2022 Jun 15];10:1–14. Available from: https://www.nature.com/articles/s41467-019-13150-0

197. Wolterink-Donselaar IG, Meerding JM, Fernandes C. A method for gender determination in newborn dark pigmented mice. Lab Anim 2009 381 [Internet]. Nature Publishing Group; 2009 [cited 2021 Dec 9];38:35–8. Available from: https://www.nature.com/articles/laban0109-35

198. Young MD, Behjati S. SoupX removes ambient RNA contamination from droplet-based single-cell RNA sequencing data. Gigascience [Internet]. Oxford University Press; 2020 [cited 2021 May 28];9:1–10. Available from: http://orcid.org/0000-0003-0937-5290

199. Germain P-L, Lun A, Garcia Meixide C, Macnair W, Robinson MD, Gartner ZJ, et al. Doublet identification in single-cell sequencing data using *scDblFinder*. F1000Research 2022 10979 [Internet]. F1000 Research Limited; 2022 [cited 2022 Jun 15];10:979. Available from: https://f1000research.com/articles/10-979

200. Hao Y, Hao S, Andersen-Nissen E, Mauck WM, Zheng S, Butler A, et al. Integrated analysis of multimodal single-cell data. Cell. Cell Press; 2021;184:3573-3587.e29.

201. Jew B, Alvarez M, Rahmani E, Miao Z, Ko A, Garske KM, et al. Accurate estimation of cell composition in bulk expression through robust integration of single-cell information. Nat Commun 2020 111 [Internet]. Nature Publishing Group; 2020 [cited 2022 Jun 7];11:1–11. Available from: https://www.nature.com/articles/s41467-020-15816-6